OPTIMIZATION OF 2D PHOTONIC CRYSTAL WAVEGUIDE USING DISPLACEMENT AND NARROWING TECHNIQUE

By

Nashad Sharif

Md. Mahbub Alam

A Thesis submitted for the degree of Bachelor in Science

BRAC UNIVERSITY

Department of Electrical and Electronic Engineering

Supervisor at BRAC University

Dr. Belal Bhuian

Acknowledgements

This thesis would not have been realized without the support and help from a lot of people. First of all, we would like to thank our advisor at the BRAC University, Dr.Belal Bhuian for his continuous guidance, support and encouragement during the work of this dissertation. He has been very helpful supplying us the necessities with the knowledge and background of the photonic crystal subject, required computer software, guided us in accomplishing the goal of our thesis work. It has been a pleasure for us to work under the supervision of our teacher into the most active and interesting research field about optical waveguide and photonic crystal. He has been very kind and would always like to discuss with us with great patience whenever we faced challenges and difficulties. Especially, he always motivated us to be active in mind and provided us many chances to broaden our views. We are also grateful to Fahmid Wasif for his continuous help.

Finally, we would like to express our loving thanks to our family. Without their understanding and support it would have been impossible for us to finish the thesis.

Abstract

In this thesis, an approach to analyze PhC structures has been developed. This approach is based on the ***displacement and narrowing*** technique. The motive is to design and optimize the desired photonic crystal waveguides and to optimize the transmission loss. Firstly, a Z -shape, a Y-shape and a Mach Zehnder photonic crystal waveguide is designed and then the designs are optimized applying the ***displacement and narrowing*** technique. The displacement method allows altering positions of certain PhC rods/atoms, thus breaking the periodicity of the rods, which is known as the displacement of the PhC rods. The narrowing technique is mainly applied to alter the characteristics of the PhC rods/atoms, which basically implies that, it allows altering the shape or pattern of the PhC rods by changing its radius, width and other certain parameters. So basically, the parameters of the PhC rods have been modified according to the requirements. Then, the PhC waveguides have been fine-tuned by displacing these narrowed rods in the bending regions of the designed PhC waveguides. The resulting wave propagation through the optimized waveguide showed that relatively small design areas were enough to yield the wanted improvement in efficiency and the numerical results obtained have shown much improved transmission. The design has been realized in a gallium-arsenide photonic crystal structure. The whole design and simulation process including PhC band gap simulation and wave propagation analysis is done using the software RSOFT.

Table of Contents

CHAPTER 4

CHAPTER 5

List of Figures

Chapter 1

Introduction

A new class of materials affects a photon's properties in much the same way that a semiconductor affects an electron's properties. The ability to mold and guide light leads naturally to novel applications in several fields, including optoelectronics and telecommunications. Presently, in telecommunications and optoelectronics, there is a great drive towards miniaturizing optical devices to the point where we are approaching the scale of the wavelength itself. The goal is eventually to integrate such devices onto a single chip. To achieve such localization, however, it might be necessary to exploit mechanisms that go beyond index guidance (total internal reflection). Growing interests have been shown in recent years in the design and optimization of photonic crystal based components such as waveguides, lasers, splitters, fibers, etc.

Generally speaking, investigation in the area of photonic crystal is expanding and a great number of research results have appeared in the last two decades, although the most successful practical application of PhCs is only photonic crystal fibers. However, much work still focuses on improving the property performance of PhCs. Photonic Crystals (PhCs) are periodic dielectric structures. They are called crystals because of their periodicity and photonic because they act on light. The optical properties of periodic structures can be observed throughout the natural world, from the changing colors of an opal held up to the light to the patterns on a butterfly's wings. Nature has been exploiting photonic crystals for millions of years, but humans have only recently started to realize their potential.

The most important discovery of this type of photonic crystal structures is the existence of photonic band gap. This is a forbidden gap for photons. Light cannot enter this region as well as electrons cannot emit photons. In other words, photonic band gap is an insulator of light. Among several importance of the photonic crystal waveguide, the key roles are the ability to obtain photonic crystals with refractive indices, the ability to control spontaneous emission in photonic crystal, to modify the state density and group velocity, to locate light by structure defects (impurity), and because of the photonic band gap and artificially introduced defects, photonic crystals are having various scientific and engineering applications in modern technology.

Photonic crystal waveguides have been a topic of extensive research for quite some time now. Several methods of optimization of photonic crystal structures have been proposed by researchers, including topology optimization approach *[1]*, geometry projection method *[2]*, simulated annealing and the finite-element method *[3]*, multiple multipole method *[4]*, etc. This thesis discusses the optimization and simulation of various types of photonic crystal waveguides by the displacement and narrowing of the air rods in gallium arsenide. The work in this thesis paper is majorly based on the concept of photonic band gaps (PBG).

This thesis comprises of four more chapters that follow, Chapter 2 gives an overview on the background of photonic crystal and discusses about its physical properties and the different types of photonic crystal structure, the physical origins of a band gap in a photonic crystal and their ability to guide waves around tight bends. This has been done to give basic knowledge about photonic crystals which should help to understand further chapters in the thesis.

Chapter 3 explains about the computational methods used for photonic crystals and gives a brief description on the modeling tools that has been used for the simulation and analysis of the respective optimized photonic crystal waveguides.

Chapter 4 is the most essential chapter of this thesis which contains an elaborated focus on the work of this thesis. This chapter gives detailed description on the design and optimizations of the Z, Y and Mach Zehnder defects and also summarizes the ***displacement and narrowing*** method, which is the optimization process that has been used to optimize the basic Z, Y and Mach Zehnder PhC structures. A section in this chapter is dedicated to the analysis and optimization of transmission loss and evidences showing a better ouput.

Chapter 5 is the final chapter of this thesis, where conclusions are drawn and possible future prospect in this field is suggested.

Chapter 2

Background and Overview on Photonic Crystals

"Photonic Crystals" (PC) are dielectric structures with periodic spatial alternations of the refractive index on the scale of the wavelength of the light. Due to this periodicity, a photonic band gap (PBG) is formed and the propagation of electromagnetic waves is prohibited for all wave vectors within this band gap. Over the past several years, various important scientific and engineering applications such as the control of light emission and propagation and the trapping of photons have been realized the photonic band gap and artificially introduced defects. Photonic crystals are a class of photonic devices that utilize periodic structures to create photonic band gaps, analogous to the III-V compound semiconductors in which photons with specific energies cannot be transmitted through the structures. The periodicity of photonic crystals can be formed by differences in dielectric constant, or by a combination of metal and dielectric, and hence the term metallodielectric photonic crystals.

2.1 – History and Introduction to Photonic Crystals

This chapter is intended as a brief overview of the history, concepts and characteristics and application of photonic crystals. Although, a single chapter is insufficient to review a field that continues to grow almost exponentially, nevertheless much is focused on the most relevant aspects of the work presented in the remainder of this thesis.

Physics of crystalline materials now is one of the most developed parts of natural science. In 1887, Lord Rayleigh first discovered the peculiar refractive properties of a crystalline mineral

with periodic “twinning” plans (across which the dielectric tensor undergoes a mirror flip). From this observation he realized there is a narrow band of wavelengths for which light propagation was prohibited through the planes *[5]*. Although, it was not until one hundred years later when John and Yablonovitch combined the theoretical tools of modern electromagnetism and solid state physics, in 1987, that research in photonic band gap established and thrived *[6]* . This generalization, which inspired the name “Photonic crystal” for structures demonstrating photonic band gaps, led to many subsequent developments in theory, fabrication and application *[7]*.

It has been shown that the spontaneous emission rate of the atoms in the media can be affected by the changing of the optical properties of the media and the emission rate can be enhanced due to coupling with the resonant states *[8]* or can be forbidden if no light states are available for the given frequency *[9]*.

In terms of dimensionality, photonic crystals can be classified into three categories: one - dimensional, two –dimensional, three-dimensional photonic crystals.

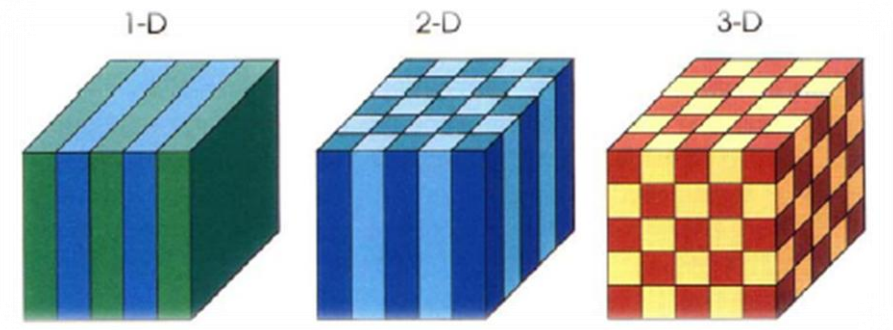

Figure 2.1.1 - Periodically in 1-D, 2-D, 3-D

Theoretically a PC can be considered as an optical analogue to the semiconductor crystal lattice which provides a periodic potential to an electron propagating through it. Hence Bragg like diffraction energy bandgaps is introduced to explain the electrons forbidden phenomenon. The electron bandgap is an energy range where there are no electrons stable. The electron bandgap is due to the periodic lattice of the atoms in semiconductor. Similarly in a PC, if the dielectric constant of the materials forming the crystal is varied periodically, the scattering at the interface can produce photonic bandgaps, thus preventing light from propagating in certain directions with specific energies (Figure 2.1.2). Photonic bandgap is a frequency gap where there is no photons existing in this range in the PC structures. This is due to the destructive interference of the light in the periodic structure.

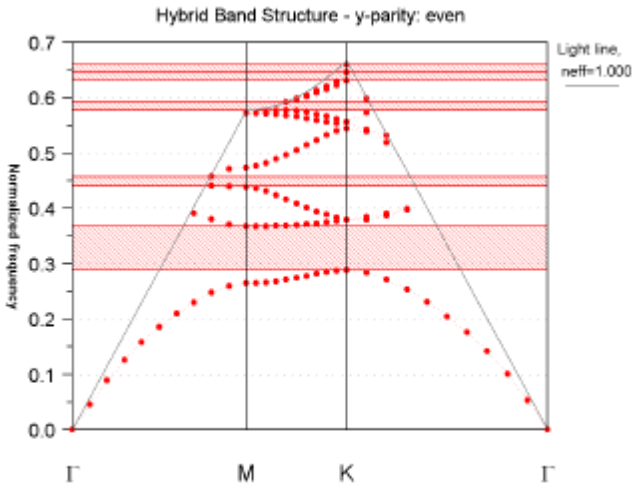

Figure 2.1.2: Photonic band gap

2.2 - One Dimensional Photonic Crystal

The simplest possible photonic crystal, shown in fig 2.1, is the one dimensional (1-D) structure. Although the term photonics crystal term is relatively new, simple one dimensional PhCs in the form of periodic dielectric stacks have been used for a long time. This is the simplest type of photonic crystal and it allows us to introduce many important properties of photonic crystal which will be used later on. One dimensional photonic crystal are consisted of alternating layers of two types of material with different dielectric constants with each pair of layers being identical with the previous or the next layer. For developing an understanding of this structure is to allow a plane wave to propagate through the material and consider the multiple reflections and transmissions that take place at each interface, then the phase changes that occur for plane waves to propagating from layer to layer. So , based on this concept a matrix method has been introduced by Yeh to treat the phenomenon of electromagnetic waves propagating through media , which actually laid the very foundation for numerical research .for one dimensional PhCs*[10]*.

The wavelength selective reflection properties of a one dimensional photonic crystal are used in wide range of off applications including high efficiency mirrors, Fabry-Perot cavities, optical filters and distributed feedback lasers. In contrast to two and three dimensional PhCs, 1D Bragg reflection occurs regardless of the index contrast; although a large number period is required achieve a high reflectance if the contrast is small. Since the absorption in dielectric

materials is very low, mirrors made from dielectric stacks are extremely efficient. The main limitation of these dielectric mirrors is that they only operate for a limited range of angles close to normal incidents.

As 1-D PhCs are the simplest photonic crystal structures and have the advantages of being easy to simulate and fabricate, they have attracted much interest both numerically and experimentally since the early days of research into PhCs. Notably, the formation of 1-D PhC integrated waveguide working as micro cavities by etching holes in a ridge waveguide has been carried out by many researchers with Villeneuve and Foresi first reporting theoretical and experimental investigations *[11].*

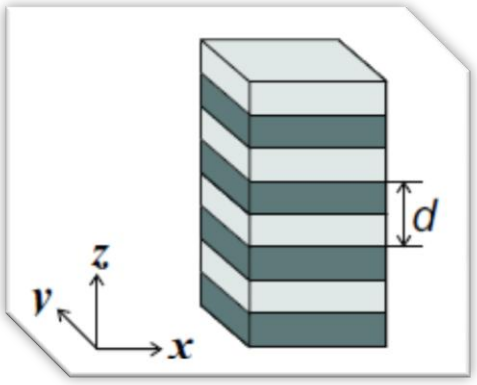

Figure 2.2- Schematic of a one dimensional photonic crystal consisted of periodic stack of dielectric layer with period d.

2.3 – Two Dimensional Photonic Crystal

Both two-dimensional (2D) and three-dimensional (3D) PhCs can be thought of Generalizations to the 1D case where a full 2D or 3D band gap appears only if the 1D Bragg reflection condition is satisfied simultaneously for all propagation directions in which the structure is periodic. For most 2D periodic lattices this occurs providing the index contrast is sufficiently large, but for 3D structures only certain lattice geometries display the necessary properties, and only then for large enough index contrasts.

In two-dimensional photonic crystals the permittivity is modulated in two directions, for example, in the (xy) plane: $\varepsilon(r) = \varepsilon(x; y)$. Any period R can be represented as R = m1a1 + m2a2 + m3a3, where aj are translation vectors, which form the basis of the photonic crystal lattice. mj are integer numbers. For the 2D photonic crystals a1 and a2 are in the (xy) plane and a3 can be chosen to be in the z direction. Because the permittivity is constant along the z direction the length of a3 can be chosen arbitrarily, it doesn't affect the results. After the identification of one-dimensional band gaps, it took a full century to add a second dimension, and three years to add the third. It should therefore come as no surprise that 2-D systems exhibit most of the important characteristics of photonic crystals, from nontrivial Brillouin-zones to topological sensitivity to a minimum index contrast, and can also be used to demonstrate most proposed photonic crystal devices *[12]*.

A second class of 2D PhC applications exploits the unique properties of the propagating modes that exist outside the band gaps in defect-free PhCs. The discrete translational symmetry of PhCs imposes strict phase conditions on the field distributions that they support. As a result, only a discrete number of modes are supported for any given frequency and light propagating in these Bloch modes can have very different properties to light in a homogeneous medium.

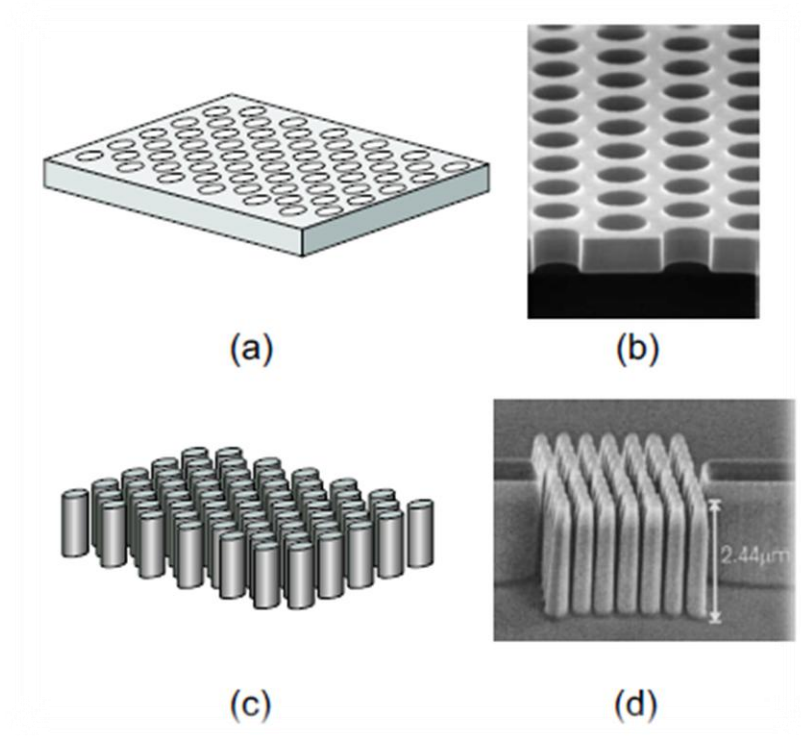

Figure 2.3: (a) Schematic of a 2D hole-type PhC slab consisting of low refractive index cylinders in a high-index slab. (b) Scanning electron microscope (SEM) image of a fabricated

hole-type PhC in a silicon slab (c) Schematic of a 2D rod-type PhC consisting of high refractive index cylinders in a low-index background. (d) SEM image of a fabricated rod-type PhC formed from GaAs rods on a low-index aluminum oxide layer.

An important parameter of the photonic crystal is the filling factor which is defined as the fraction of the photonic crystal primitive cell area occupied by the photonic crystal “atoms". This parameter reflects the coupling strength of the light and the photonic crystal and greatly affects the Bloch mode dispersion properties.

2.4 – Three Dimensional Photonic Crystal

Three-dimensional PhCs have proved to be the most challenging PhC structures to fabricate. Whereas 2D PhC research has gained significant benefit from well established 1D PhC thin-film and semiconductor processing technology such as plasma deposition and electron-beam lithography, fabrication of 3D PhCs has required the development of entirely new techniques. For this reason, it was more than three years after the initial proposal for 3D band gap materials *[13]* before a structure was calculated to exhibit a band gap for all directions and all polarizations *[14]*. The design consisted of dielectric spheres positioned at the vertices of a diamond lattice. This followed experimental reports the previous year in which a partial band gap in a face-centered- cubic (FCC) lattice of spheres was mistakenly identified as a complete band gap *[15]***.** This latter result highlighted the requirement for rigorous theoretical and computational tools capable of dealing with high-index contrast dielectrics.

Three dimensional photonic crystals were at the origin of the very notion of photonic crystal, and it is believed that only photonic crystals presenting a three-dimensional periodicity are capable of providing an Omni directional band gap with the complete suppression of the radiative states in the corresponding frequency range *[16]*. The first three dimensional PhC possessing a Photonic Band Gap was fabricated by Yablonovitch et al *[17]* at microwave frequencies and is known as “Yablonovite”. The fabrication technique involved covering a slab of dielectric with a mask consisting of a triangular array of holes. Each hole is drilled through three times at an angle 35.26°away from the normal and spread 120°in azimuth. The relative size of the photonic band gap, i.e. the gap frequency divided by the mid-gap frequency, was found to be around 21%, which agrees well with theory *[18]*.

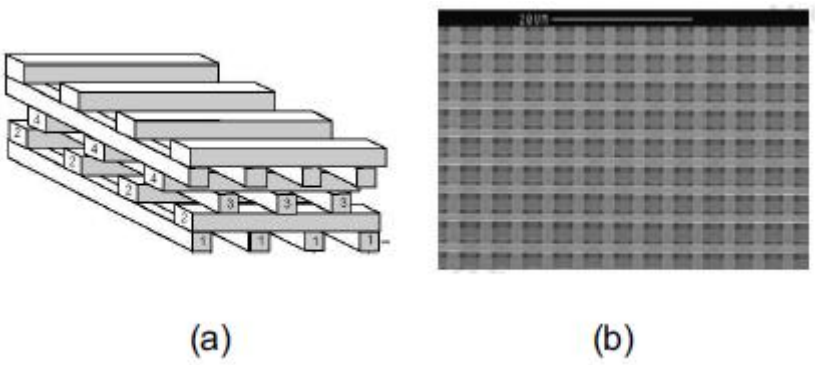

Figure 2.4: An example of a 3D PhC woodpile structure known to exhibit a full photonic Band gap. (a) Schematic of an ideal woodpile PhC. (b) SEM image of a real 3D woodpile structure fabricated in silicon.

2.5 – Application of Photonic Crystals

The study of material properties has lead to many breakthroughs in Science. Prehistoric ancestors have intelligently acquired the skill of extracting materials from nature, studying its physical properties to fashion tools for their survival. Eventually, humankind wanted more than just the raw form of materials. Scientists and engineers began tempering with existing ones to create new materials with even more superior properties such as stainless steel, ceramics, etc. Today, a wide variety of artificial materials with excellent physical and chemical properties is in possession. In this century, control over materials has extended to include their electrical and magnetic properties. Advances in semiconductor physics have permitted to modify conductivity, permeability of materials, thereby pioneering the unprecedented age of transistors and integrated circuits. Even more recently, graphene has proven itself to be a novel material with phenomenal electrical conductivities and transport regimes. In the last decade, a new frontier has emerged with a similar goal: to control the optical properties of materials. Scientists and engineers desire to fabricate materials with the ability to selectively prohibit light, direct light or even localize light in desired regions. All these are easily accomplished with the help of photonic crystals. As such, photonic crystals have earned their place in science and technology advances today.

The ideas of photonic crystal are very exciting but the hard truth is realization is not. A rule of thumb is that the lattice constant of the photonic crystal is about one half to one third of wavelength. Even the wavelength we choose is at the infrared range, say 1.5 μm, this means a lattice constant about 0.5 to 0.8 μm. And the features inside the cell should be even smaller in dimension, about 0.2 to 0.4μm. This is nearly the technological limit of current best microlithography techniques. The electron beam lithography and X-ray lithography are two candidates for improved fabrication of such small features.

The applications of PBG structures include the design of ultra-compact lasers that emit coherent light with almost no pumping threshold, all-optical switching fabrics for routing data along the internet, single atom memory effects for quantum computer applications and all-optical transistors. Owing to their unique ability for controlling photon transmission, PhCs are predicted to have many applications in future optical and photonic systems, stimulating much work aimed at demonstrating practical devices.

2.5.1 –Waveguides

One very promising application of PhCs is aimed at improving the performance of waveguides *[19]* although optical fibers guide light over long distances, micro-circuits of light based on waveguides do not exist. PBG materials remove this problem by removing all the background electromagnetic modes over the relevant band of frequencies. Now, when a light is shone on the crystal it has nowhere else to go and so it traces the path of the defect. The PBG localizes the light and prevents it from escaping the optical micro-circuit. Even through a 90o bend, 98 % of the power in the light that goes in one end comes out of the other.

Guiding and trapping light using waveguides and resonant cavities are two fundamental optical functions that enable a range of all-optical devices to be created. Waveguides not only perform the tasks of their electrical analogues, wires, by transferring light from one part of a circuit to another, but are used in many other devices such as couplers, junctions and interferometers. Resonant cavities have many potential applications that make use of the sharp spectral response and very strong field intensities that occur at resonance. There are various

methods for achieving efficient wave guiding and many others for producing high quality optical cavities, but very few single technologies allow both to be engineered in a single integrated structure. Two dimensional photonic crystals can provide just such a combination due to their versatile geometry that allows simultaneous fine tuning of a number of parameters. *[20]* 3D PhCs could potentially provide even greater control over light, but they are considerably more challenging to fabricate. In addition, the complex lattice structures required to achieve full 3D band gaps can make it very difficult to create high quality defects. The possibility of producing cavities and waveguides in PhCs by introducing defects was recognized not long after the first 2D band gap structures were proposed. In 1994, Meade et al. suggested that both cavities and waveguides could be created in 2D PhCs by simply changing or removing a single cylinder or a whole line of cylinders, respectively. A defect created in this way is surrounded by the uniform PhC that acts as an Omni directional mirror for light at frequencies in the band gap, thus trapping light in the defect region. In a cavity defect, this can result in sharp resonant behavior, whereas a linear defect allows light to propagate along the defect while being confined in the transverse direction by perfectly reflecting PhC walls. In a PhC slab, this is only true for light confined vertically by TIR, but the behavior is essentially the same.

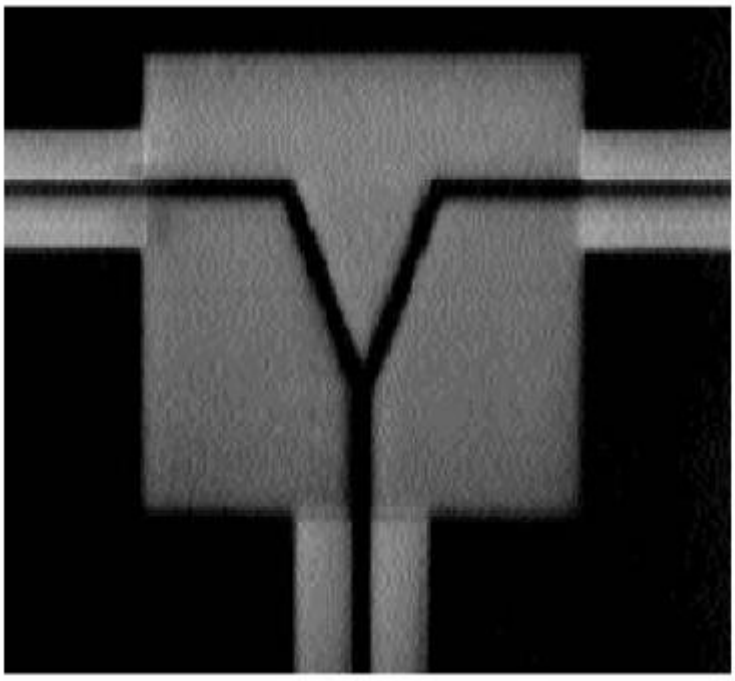

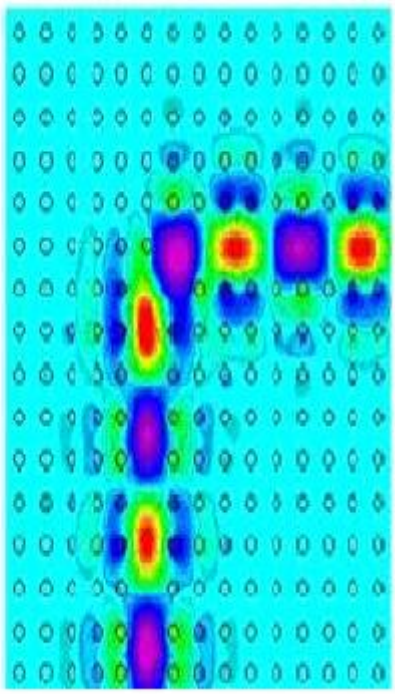

Figure 2.5.1 : Line defect in a photonic crystal Left: A beam splitter photonic crystal Right: electric field of light propagating down a waveguide with a sharp bend carved out of a square lattice of dielectric rods.(Courtesy of Ouellette.)

2.5.2 - Photonic Crystal Fibers

Photonic Crystal Fibers (PCFs) are optical fibers that employ a micro structured arrangement of low-index material in a background material of higher refractive index. The background material is often un-doped silica and the low index region is typically provided by air voids running along the length of the fiber. PCFs may be divided into two categories, high index guiding fibers and low index guiding fibers. High index guiding fibers are guiding light in a solid core by the Modified Total Internal Reflection (M -TIR) principle. The total internal reflection is caused by the lower effective index in the micro structured air-filled region. Low index guiding fibers guide light by the photonic band gap (PBG) effect. The light is confined to the low index core as the PBG effect makes propagation in the micro structured cladding region impossible. The strong wavelength dependency of the effective refractive index and the inherently large design flexibility of the PCFs allows for a whole new range of novel properties. Such properties include endlessly single-moded fibers, extremely nonlinear fibers and fibers with anomalous dispersion in the visible wavelength region.

2.5.3 - Add Drop Filters

An add-drop filter for a wavelength division multiplexed (WDM) communication system is depicted in Figure 2.9. Here, light from an optical fiber carrying many different frequencies, F1, F2,… is inserted into a 2D PBG structure by means of a wave guide channel (missing row of holes). The frequencies F1, F2,… lie within the 2D PBG and cannot escape from the waveguide channel except in places where the periodicity of the background pores is disrupted by means of defects. For example, a hole that is larger than all the other background holes can act as a resonator which picks off a particular frequency, say F1, from the wave guide channel, while allowing other frequencies to propagate freely along the wave guide.

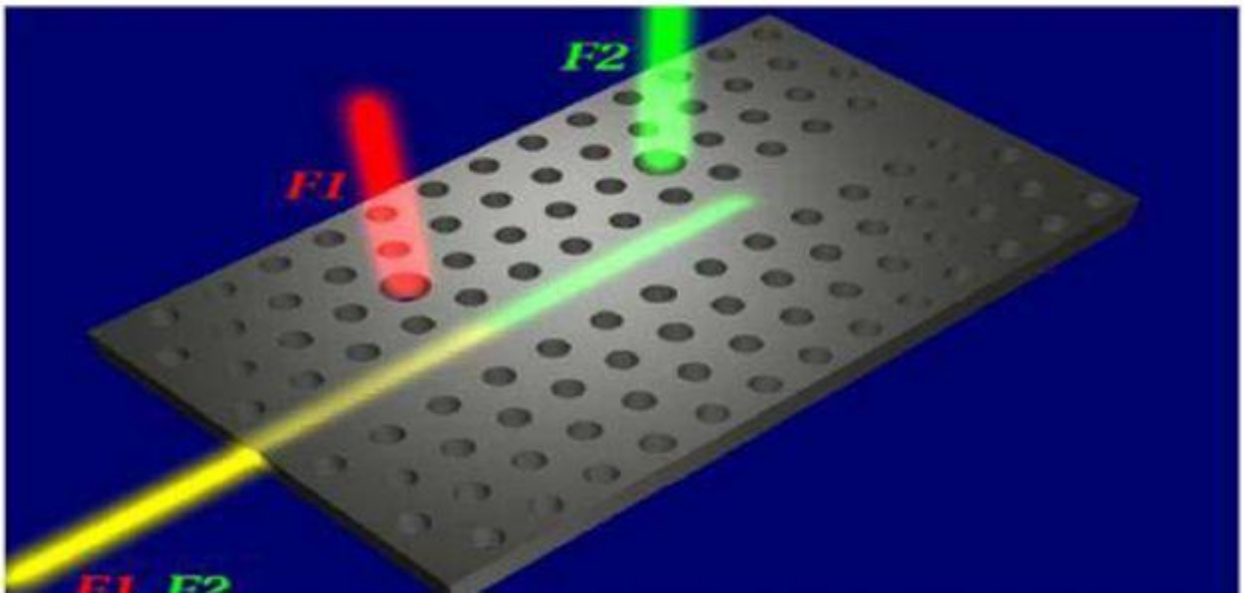

Figure 2.5.2: Add drop filters multiple streams of data carried at different frequencies F1, F2, etc. (yellow) enter the optical micro-chip. Data streams at frequency F1 (red) and F2 (green) tunnel into localized defect modes and are routed to different destinations. (Courtesy of Sajeev John, University of Toronto.)

2.5.4 – Integrated Circuits

One of the goals of photonic crystals is to create ultra small optical and optoelectronic integrated circuits as conceptualized in Fig.1.5.4. Such devices integrate nano-ampere laser arrays with different oscillation frequencies, waveguides that incorporate very sharp bends, optical modulators, wavelength selectors, and so on, all in an area less than 100 × 100 μm2. The optical devices are created by introducing appropriate artificial defects and light emitters in the crystal.

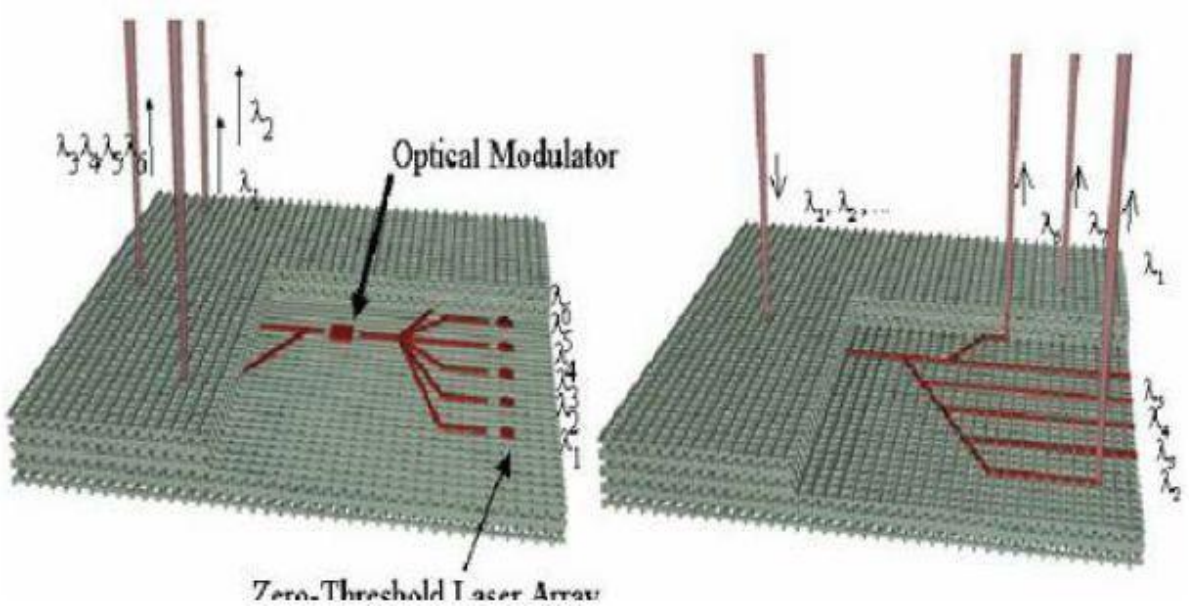

Figure 2.5.3: Integrated optic circuit an artist's conception of a 3D PBG woodpile structure into which a micro-laser array and de-multiplexing (DEMUX) circuit have been integrated. (Courtesy of S. Noda, Kyoto University, Japan.)

2.5.5- Tunable PBG materials

For many applications, it is advantageous to obtain some degree of tunability of the photonic band structure through electro-optic effects. This may be useful in routing of signals through an optical network and provide flexibility to reconfigure the routing as conditions in the network change. The pores in the materials can be infiltrated with other electro-optically active materials which enable reconfiguration of the underlying photonic band structure. Tunability may be obtained by controlling the optical anisotropy of the constituent materials. Inverse opal structures provide a highly efficient scattering system as illustrated by the complete PBG of silicon inverse opals. The nearly 75% empty volume of this structure is ideally suited for

infiltration by a low refractive index liquid crystal with strong optical anisotropy making them efficacious for electro optic tuning effects. In particular, a change in the orientation of the nematic director field with respect to the inverse opal backbone by an external electric field can completely open or close the full, three-dimensional PBG. This clearly demonstrates an electro-optic shutter effect to the PBG which may be realized by external means.

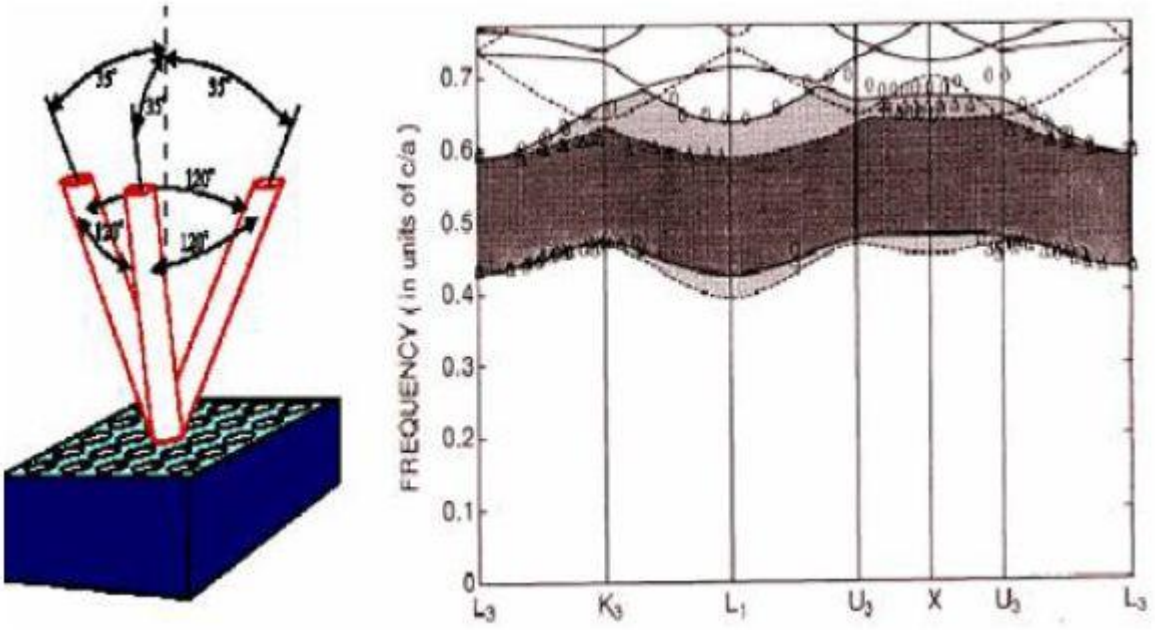

Figure 2.5.4: Yablonovite structure this is first three dimensional photonic crystals to be made and it was named Yablonovite after Yablonovitch who conceptualized it. The dark shaded band on the right denotes the totally forbidden gap (courtesy of Yablonovitch, University of California, Los Angeles.)

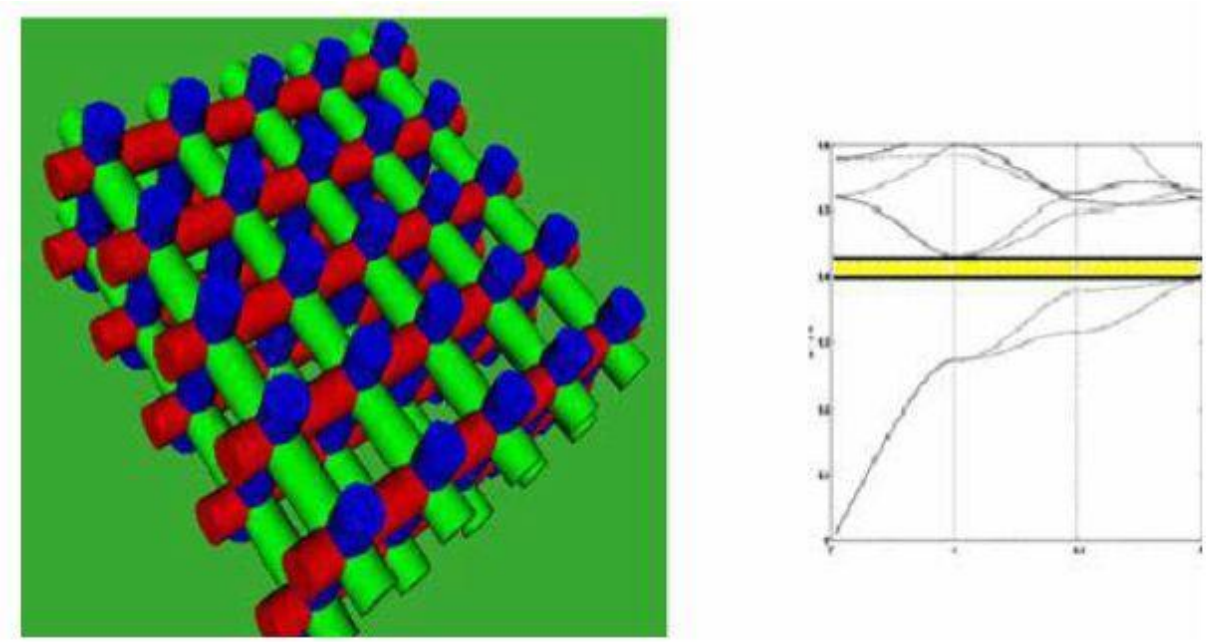

Figure 2.5.5: The scaffolding structure (for its similarity to scaffolding) is a rare example of a photonic crystal that has a very different underlying symmetry from the diamond structure yet has a photonic band gap (courtesy of Joseph Haus, Catholic university of America.)

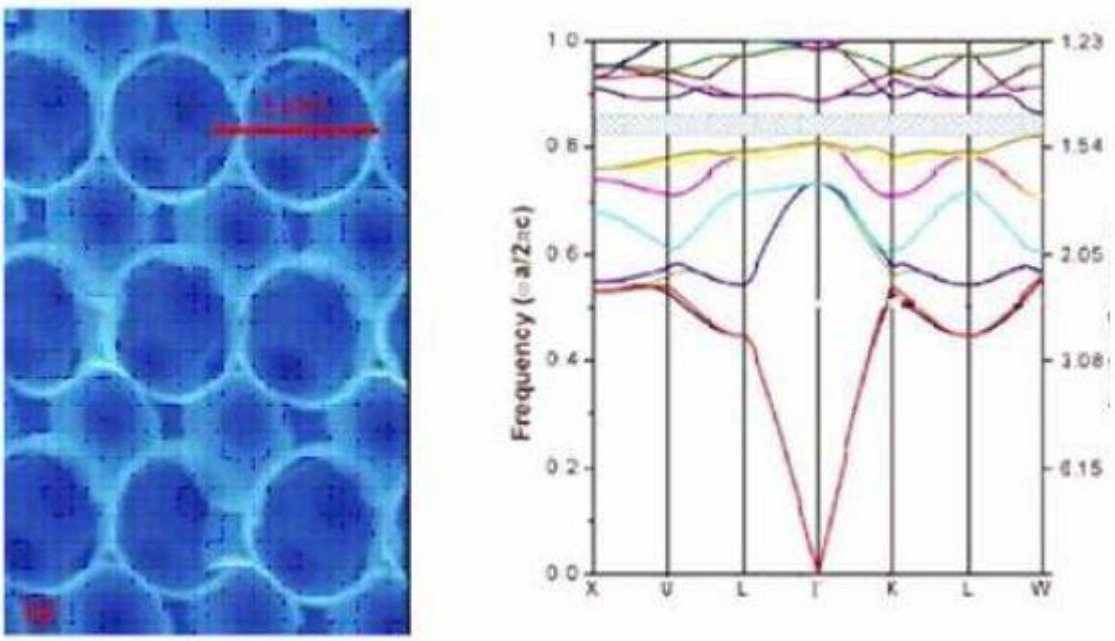

Figure 2.5.6: the inverse opal structure SEM picture of a cross-section along the cubic (110) direction of a Si inverse opal with complete 5% PBG around 1.5 um.

Chapter 3

Computational Methods of Photonic Crystal Structures

The modes of the photonic crystal must of course be solutions of Maxwell's equations. However, symmetry considerations place restrictions on the possible form of the solutions. In particular, the modes must satisfy the appropriate translation symmetry.

3.1 - The Maxwell's Equation

The investigation and study of wave propagation in periodic media was first made by Felix Bloch *[21]***.** He showed that the wave propagation in periodic media can be successfully accomplished without scattering of the waves. He proved that the wave drifting in the periodic medium is modulated by a periodic function. This periodic function is due to the periodicity of the structure of the medium, identical to the travelling of the electronic waves in the crystal structures. The identical analogue can be applied to the electromagnetic wave propagation but, here, the periodicity is in the dielectric difference of the medium. We start the mathematical analysis by Maxwell's curl equations.

$$\boldsymbol{\nabla} \times \boldsymbol{E} + \frac{\boldsymbol{\partial B}}{\boldsymbol{\partial t}} = \mathbf{0}$$

$$\boldsymbol{\nabla} \times \boldsymbol{H} - \frac{\boldsymbol{\partial D}}{\boldsymbol{\partial t}} = \boldsymbol{J}$$

(3.1)

$$\boldsymbol{\nabla} \times \boldsymbol{B} = \mathbf{0}$$

$$\nabla \times D = \rho$$

The quantities E and H are the electric and magnetic fields, measured in units of [volts/m] and [Ampere/m] respectively. The quantities D and B are the electric and magnetic flux densities respectively. In linear, isotropic and non-dispersive materials, the E and H fields, relate to electric and magnetic flux through the following equations:

$$D = \xi E = \xi o \, \xi r \, E$$

(3.2)

$$B = \mu H = \mu o \, \mu r \, H$$

Now assume no current flow or charge density in the system, then:

$$\nabla \times E + \frac{\partial B}{\partial t} = 0 \qquad (3.3)$$

$$\nabla \times H - \frac{\partial D}{\partial t} = 0$$

$$\nabla \times E = -\mu o \frac{\partial H}{\partial t}$$

$$\nabla \times H = \mathcal{E} o \, \mathcal{E} r \, \frac{\partial E}{\partial t} \qquad (3.4)$$

$$\nabla \cdot H = 0$$

$$\nabla \cdot E = 0$$

Generally, E and H are both complex functions of space and time, since the Maxwell equations are linear**,** though, from the spatial dependence**,** we can break up the time dependence by increasing the fields into a set of harmonic-modes. So the harmonic mode as a spatial prototype or "mode profile" times a complex exponential is set by:

$$H(r,t) = H\,(r)\, \mathrm{e}^{-i\omega t}$$

(3.5)

$$E(r,t) = E\,(r)\, \mathrm{e}^{-i\omega t}$$

By putting equation (3.5) in equation (3.4), the two divergence equations are given by:

$$\boldsymbol{\nabla \cdot H(r) = 0}$$

(3.6)

$$\boldsymbol{\nabla \cdot E(r) = 0}$$

The two curl equations relate E(r) to H(r) is:

$$\boldsymbol{\nabla \times E(r) = - i\omega\, \mu o\, H(r)}$$

(3.7)

$$\boldsymbol{\nabla \times H(r) = \; i\omega\, \varepsilon o\, \varepsilon r\, E(r)}$$

If we divide the magnetic curl equation in equation (3.7) by εr and take the curl, we obtain the following equation, called the master equation *[22]***.**

$$\boldsymbol{\nabla \times \left(\frac{1}{\varepsilon r} \nabla \times H(r)\right) = \left(\frac{\omega}{c}\right)^2 \times H(r)} \qquad (3.8)$$

Where $\boldsymbol{\varepsilon r}$, is the dielectric constant and is function of the position. Equation (2.8) is an Eigen value equation, with Eigen value $\left(\frac{\omega}{c}\right)^2$ (ω are real (lossless)) and an Eigen operator $\left(\nabla \times \frac{1}{\varepsilon}\right)$ which is called Hermetian operator. H(r) is the Eigen state, and the Eigen states are orthogonal. The two curls gives "kinetic energy" and $\frac{1}{\varepsilon}$ gives the "potential energy", compared to the Hamiltonian in Schrodinger equation.

The equation given above is a slightly different form of Maxwell's equation. For the derivation of any standard wave equation, we do the similar procedure. We can also express the master equation (ME) is terms of electric field, but expressing it in terms of magnetic field H, because it has a series of properties that has got very important physical consequences and

these properties are relatively easily to derive. By expressing the master equation in the Eigen value equation as:

$$\boldsymbol{\Theta H(r)} = \left(\frac{\omega}{c}\right)^2 \times \boldsymbol{H(r)} \qquad (3.9)$$

$$\boldsymbol{\Theta H} = \boldsymbol{\nabla} \times \left(\frac{1}{\varepsilon} \boldsymbol{\nabla} \times \boldsymbol{H}\right) \qquad (3.10)$$

The condition for the E-field is:

$$\boldsymbol{\nabla} \times \boldsymbol{\nabla} \times \boldsymbol{E(r)} = \left(\frac{\omega}{c}\right)^2 \boldsymbol{\xi r}\ \boldsymbol{E(r)} \qquad (3.11)$$

It is referred to as a generalized Eigen problem, since there are operators on both sides of this equation. It is an easy matter to change this into a normal, Eigen problem by dividing equation (2.11) by $\boldsymbol{\xi}$, but then operator is not a Hermitian.

We can reinstate a simpler transversality constraint by using D in place of E, since $\nabla . D = 0$.

Putting $\frac{D}{\boldsymbol{\xi o}\ \boldsymbol{E}}$ for E in equation (2.11) and, to keep the operator Hermitian, divide both sides by $\boldsymbol{\xi}$ which yields:

$$\frac{1}{\xi(\mathbf{r})} \boldsymbol{\nabla} \times \boldsymbol{\nabla} \times \frac{1}{\xi(\mathbf{r})} \mathbf{D(r)} = \left(\frac{\omega}{\mathbf{c}}\right)^2 \frac{1}{\xi(\mathbf{r})} \mathbf{D(r)} \qquad (3.12)$$

This equation looks like being much more complex, so we prefer the “H” for numerical calculations.

3.2- Bloch's Theorem

Similar to traditional crystals of atoms or molecules, photonic crystals do not have continuous translational symmetry. They have (photonic crystal) discrete translational symmetry i.e. under translations of any distance they are not invariant but, instead, just distances, which are the multiples of certain fixed step lengths *[23]*.

In photonic crystals, the wave propagates according to the Bloch's theorem. The propagation is a function of a periodicity in the medium. In optical periodic media (photonic crystals), there is a periodic variation in dielectric constants. The refractive indices are functions of positions.

$$\boldsymbol{\mathcal{E}(x) = \mathcal{E}(x + a)}$$

$$\boldsymbol{\mu(x) = \mu(x + a)} \qquad \textit{(3.13)}$$

Where, 'a' is any arbitrary lattice vector. The above equations state that the medium repeats its properties after position 'x+a'. The Bloch's theorem is given by:

$$\overrightarrow{\boldsymbol{H}}\,(\overrightarrow{\boldsymbol{x}}, \boldsymbol{t}) = \boldsymbol{e}^{\boldsymbol{i}\left(\overrightarrow{\boldsymbol{k}}\cdot\overrightarrow{\boldsymbol{x}} - \boldsymbol{\omega t}\right)}\,\overrightarrow{\boldsymbol{H}}_{\vec{\boldsymbol{k}}}(\boldsymbol{x}) \qquad \textit{(3.14)}$$

Where $\boldsymbol{e}^{\boldsymbol{i}\left(\overrightarrow{\boldsymbol{k}}\cdot\overrightarrow{\boldsymbol{x}} - \boldsymbol{\omega t}\right)}$ is a plane wave, and $\overrightarrow{\boldsymbol{H}}_{\vec{\boldsymbol{k}}}(\boldsymbol{x})$ is periodic "envelop". K is conserved, i.e. no scattering of Bloch wave occurs ω are discrete $\boldsymbol{\omega}_{\boldsymbol{n}\,(\boldsymbol{k})}$. It is important to know that Bloch state having wave vector 'k', and the Bloch state having waved vector 'k+mc', are the same. So the k's that are different by integral multiples of $= 2\pi/a$, are not distinct from the physical point of view. Therefore, the frequencies of mode should also be periodic in k. K exists in the range $-\frac{\boldsymbol{\pi}}{\mathbf{a}} < \mathbf{k} < \boldsymbol{\pi}/\mathbf{a}$. This area of imperative, non-redundant values of k is known as the Brillouin

zone. The shortest area inside the Brillouin zone, for which the $\boldsymbol{\omega_{n\,(k)}}$(frequency bands) are not linked by symmetry, is known as irreducible Brillouin zone. The irreducible Brillouin zone consists of a triangular block with 1/8 the area of the complete Brillouin zone, and the remainder of the zone contains redundant versions of the irreducible zone.

When the dielectric is periodic in three dimensions, then dielectric is invariant in that case under translations through a large number of three dimensional lattice vectors R. These vectors can be inscribed as a specific arrangement of the three primitive lattice vectors, (a1, a2, a3), that are called to "span" the space of lattice vectors, or each R= la1+ma2+na3 for various integers l, m, and n, the vectors (a1, a2, a3) provide three primitive reciprocal lattice vectors (c1, c2, c3) So that

$$\boldsymbol{a_j \cdot c_j = 2\pi\, \delta_{i\cdot j}} \qquad (3.15)$$

These reciprocal vectors span a reciprocal lattice of their individual that is occupied by the wave vectors. The modes of a 3D periodic system are Bloch states that can be marked by a Bloch wave vector

$$\boldsymbol{K = k1c1 + k2c2 + k3c3} \qquad (3.16)$$

Where, "K" is in the Brillouin zone. Every value of the wave vector K within the Brillouin zone recognizing an Eigen state of $\boldsymbol{\nabla \times \frac{1}{\varepsilon} \nabla \times}$ with $frequency\ \boldsymbol{\omega(k)}$ and an Eigen vector $\boldsymbol{H_k}$ of the type

$$\boldsymbol{H_k(r) = e^{ik\cdot r} \cdot u_k(r)} \qquad (3.17)$$

Where $\boldsymbol{u_k(r)}$, a periodic function of the lattice is: $\boldsymbol{u_k(r) = u_k(r + R)}$,for each lattice vectors R.

3.3-The First Brillouin Zone

Brillouin zones are an important characteristic of crystal structures. The construction and illustration of Brillouin zones for a three dimensional lattice are somewhat difficult to follow. The construction of Brillouin zones for a two dimensional lattice is much easier to follow.

A Bragg *plane* for two points in a lattice is the plane which is perpendicular to the line between the two points and passes through the bisector of that line. The first Brillouin zone for a point in a lattice is the set of points that are closer to the point than the Bragg plane of any point. In other words one can reach any of the points in the first Brillouin zone of a lattice point without crossing the Bragg *plane* of any other point in the lattice.

The second Brillouin zone is defined as the points which may be reached from the first Brillouin zone by crossing only one Bragg "plane." This can be generalized to define the n-th Brillouin zone as the set of points, not in the previous zones, that can be reached from one (n-1) th zone by crossing one and only one Bragg plane.

In constructing the Brillouin zones for a point it is expedient to first determine the nearest neighbors, the next nearest neighbors and so on. This is conveniently illustrated with a square lattice. Shown below are the nearest through fourth-nearest neighbors and their Bragg lines.

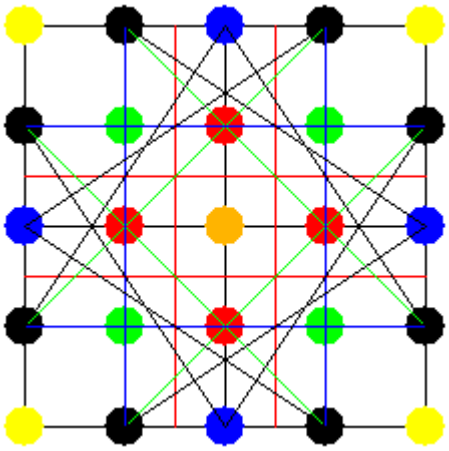

Figure 3.1: the nearest through fifth nearest neighbors for a point in their Square lattice and their Bragg lines.

The zones can easily be determined from their definitions. The first zone, one within all of the Bragg lines is shown red below. The second zone is all the points that can be reached by crossing one and only one Bragg line from the first zone. The second zone is shown in green in the illustration below. The third zone, shown in blue, consists of all the points that can be reached by crossing only one Bragg line from the second zone. The fourth zone is shown in black.

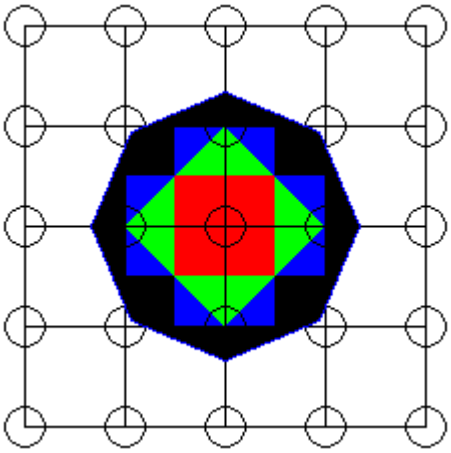

Figure 3.2: First four Birillouin zones for a square lattice.

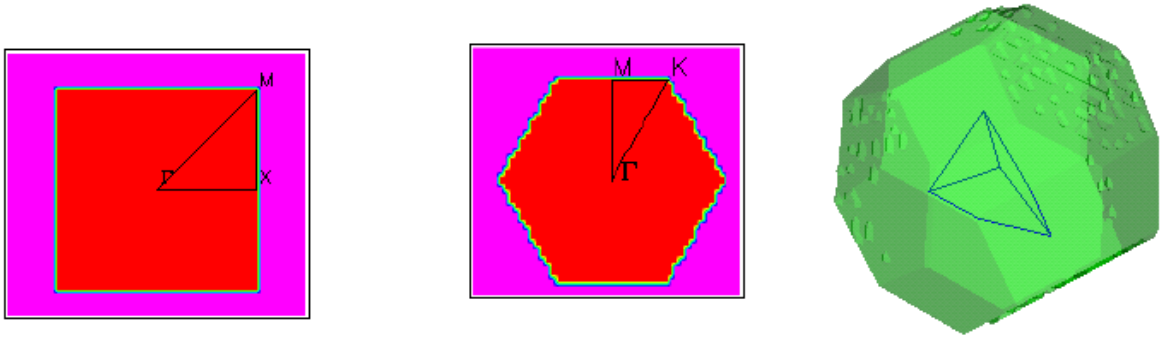

Figure 3.3: First Brillouin zones for several crystals. a) 2D square lattice, b) 2D hexagonal lattice and c) 3D face-centered cubic lattice.

3.4- Computational Methods

3.4.1-Frequency Domain Method:

In the frequency-domain method, we are trying to solve the field distributions of the steady state from the Maxwell equations. The fields are expanded into a set of harmonic modes that have the following temporal characteristics:

$$\overrightarrow{\boldsymbol{H}}(\vec{\boldsymbol{r}},\boldsymbol{t}) = \overrightarrow{\boldsymbol{H}}(\vec{\boldsymbol{r}})\boldsymbol{e}^{\boldsymbol{i\omega t}} \qquad (3.18)$$

$$\overrightarrow{\boldsymbol{E}}(\vec{\boldsymbol{r}},\boldsymbol{t}) = \overrightarrow{\boldsymbol{E}}(\vec{\boldsymbol{r}})\boldsymbol{e}^{\boldsymbol{i\omega t}} \qquad (3.19)$$

After substituting the above equations (3.18) and (3.19) into the Maxwell equations (3.1) to (3.4), we can obtain the following equation for the magnetic filed H:

$$\boldsymbol{\nabla}\left(\frac{\mathbf{1}}{\boldsymbol{\varepsilon}(\vec{\boldsymbol{r}})}\boldsymbol{\nabla}\times\overrightarrow{\boldsymbol{H}}(\vec{\boldsymbol{r}})\right) = \left(\frac{\boldsymbol{\omega}}{\boldsymbol{c}}\right)^{\mathbf{2}}\overrightarrow{\boldsymbol{H}}(\vec{\boldsymbol{r}}) \qquad (3.20)$$

Equation (3.20) defines an Eigen value problem and can be solved by a variation approach. After the magnetic filed H is found, the electric field can be obtained by the following relation:

$$\vec{\mathbf{E}}(\vec{\mathbf{r}}) = \left(-\frac{\mathbf{ic}}{\boldsymbol{\omega}\boldsymbol{\varepsilon}(\vec{\mathbf{r}})}\right)\boldsymbol{\nabla}\times\vec{\mathbf{H}}(\vec{\mathbf{r}}) \qquad (3.21)$$

3.4.2-Finite-Difference Time-Domain Method (FDTD):

The Finite-Difference Time-Domain (FDTD) method, introduced by K. S. Yee in 1966 *[24]*, was as the first technique for the direct time-domain solutions to the Maxwell's curl equations in the space lattice, and has been the subject of very rapid development. Since about 1990 when engineers in the general electromagnetic community became aware of the modeling capabilities of the FDTD and related techniques, the interest in this area has expanded well beyond defense technologies, into even non-traditional electromagnetic related areas.

The FDTD method applies a set of simple central-difference approximations for the space and time derivatives of electric and magnetic fields that are second-order accurate directly to the respective differential operators of the time-dependent Maxwell's curl equations, instead of potentials, and therefore, achieves a sampled-data reduction of the continuous electromagnetic fields in a volume of space and over a period of time *[25]*. Overall, the FDTD technique is a marching-in-time procedure that simulates the actual wave in the finite space lattice by the analogous numerical wave propagation stored in the computer memory.

Finite-difference time-domain method (FDTD) has been widely used in the area of computational electrodynamics to analyze the interactions between electromagnetic waves and complex dielectric or metallic structures *[26]*. In the general procedures, finite differences are used to approximate Maxwell equations in real space and appropriate boundary conditions are imposed in order to simulate finite or infinite structures. Then the response of the structure to the electromagnetic waves in time domain can be obtained by time-marching the fields. The Maxwell curl equations are discretized on the Yee's lattice. The field's variables are defined on a rectangular grid. Electric and magnetic fields are temporarily separated by one-half time step. Also, the electric and magnetic fields are spatially interlaced by half a grid cell. Based on this scheme, finite differences in both time and space are used to approximate the Maxwell equations on each grid point.

In order to compute the field at any given grid point on a Yee's lattice, the field values at every adjacent grid point on the grid have to be known first. But with a finite computational domain, the field values from grid points outside the domain are not available. Therefore, field values on the boundaries have to be updated by using appropriate boundary conditions.

The FDTD Algorithm

Imagine a region of space where which contains no flowing currents or isolated charges. Maxwell's curl equations in can be written in Cartesian coordinates as six simple scalar equations. Two examples are:

$$\frac{\partial H_x}{\partial t} = -1/\mu\left(\frac{\partial E_y}{\partial z} - \frac{\partial E_z}{\partial y}\right) \qquad (3.22)$$

$$\frac{\partial E_y}{\partial t} = -1/\varepsilon\left(\frac{\partial H_x}{\partial z} - \frac{\partial H_z}{\partial x}\right) \qquad (3.23)$$

The other four are symmetric equivalents of the above and are obtained by cyclically exchanging the x, y, and z subscripts and derivatives. Maxwell's equations describe a situation in which the temporal change in the **E** field is dependent upon the spatial variation of the **H** field, and vice versa. The FDTD method solves Maxwell's equations by first discretizing the equations via central differences in time and space and then numerically solving these equations in software.

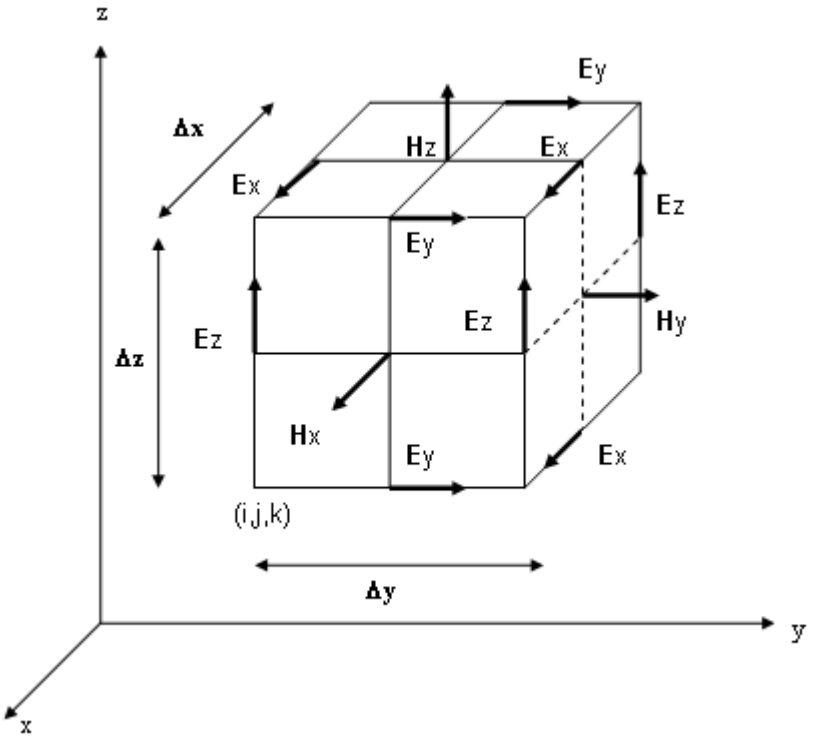

Figure 3.4 - In a Yee cell of dimension Ax, Ay, Az, note how the H field is computed at points shifted one half grid spacing from the E field grid points

The most common method to solve these equations is based on Yee's mesh and computes the **E** and **H** field components at points on a grid with grid points spaced Δx, Δy, and Δz apart. The **E** and the **H** field components are then interlaced in all three spatial dimensions as shown in Fig. 2-1. Furthermore, time is broken up into discrete steps of Δt. The **E** field components are then computed at times $t = n\,\Delta t$ and the **H** fields at times $t = (n+1/2)\,\Delta t$, where n is an integer representing the compute step. For example, the **E** field at a time $t = n\,\Delta t$ is equal to the **E** field at $t = (n-1)\,\Delta t$ plus an additional term computed from the spatial variation, or curl, of the **H** field at time t.

This method results in six equations that can be used to compute the field at a given mesh point, denoted by integers i, j, k. For example, two of the six are:

$$H^{n+1/2}_{x(i,j,k)} = H^{n-1/2}_{x(i,j,k)} + \frac{\Delta t}{\mu \Delta z}\left(E^{n}_{y(i,j,k)} - E^{n}_{y(i,j,k-1)}\right) - \frac{\Delta t}{\mu \Delta y}\left(E^{n}_{z(i,j,k)} - E^{n}_{z(i,j-1,k)}\right)$$

$$E^{n+1}_{x(i,j,k)} = E^{n}_{x(i,j,k)} + \frac{\Delta t}{\varepsilon \Delta y}\left(H^{n+1/2}_{z(i,j+1,k)} - H^{n+1/2}_{z(i,j,k)}\right) - \frac{\Delta t}{\varepsilon \Delta z}\left(H^{n+1/2}_{y(i,j,k+1)} - H^{n+1/2}_{y(i,j,k)}\right)$$

These equations are iteratively solved in a leapfrog manner, alternating between computing the **E** and **H** fields at subsequent $\Delta t/2$ intervals.

3.5: Light Propagation in Photonic Waveguide

Photonic crystal slab waveguide is formed by removing one row of air holes from the periodic lattice. This introduces a line defect inside the periodic lattice, adding guided modes inside the photonic stop band. The image of a free standing waveguide with missing-hole line defect is shown in Figure 3.3. Since our concern is the dispersion of the guided modes which are confined within the line defect, we take the original band structure and project the wave vectors onto the propagation direction. The projected band structure is shown in Figure 3.4.

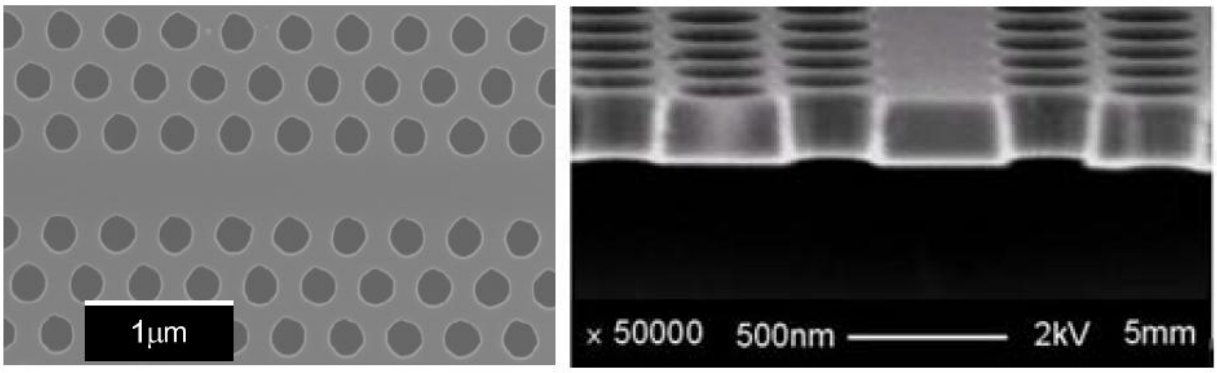

Figure 3.5.1: Photonic waveguides formed by missing -hole defect.

All the leaky modes above the light line are neglected since PWE simulation generates useful results only below the light line and the leaky modes are not our concern. Below the light line, three guided modes are usually identified: (1) the fundamental TE-like guided mode; (2) and the second order TE-like guided mode; (3) the fundamental TM-like guided mode. In this simulation, the lattice constant of photonic crystals is 400nm, the filling factor is 0.3, the refractive index is 3.5, and the slab thickness is 220nm.

This simulation used ideal photonic waveguide with perfect symmetry, and TE-like modes and TM-like modes are orthogonal as even modes and odd modes with respect to the central slab plane. However, in reality, due to the fabrication uncertainty, no waveguide is perfectly symmetric and thus TE-like modes and TM-like modes would no longer be orthogonal.

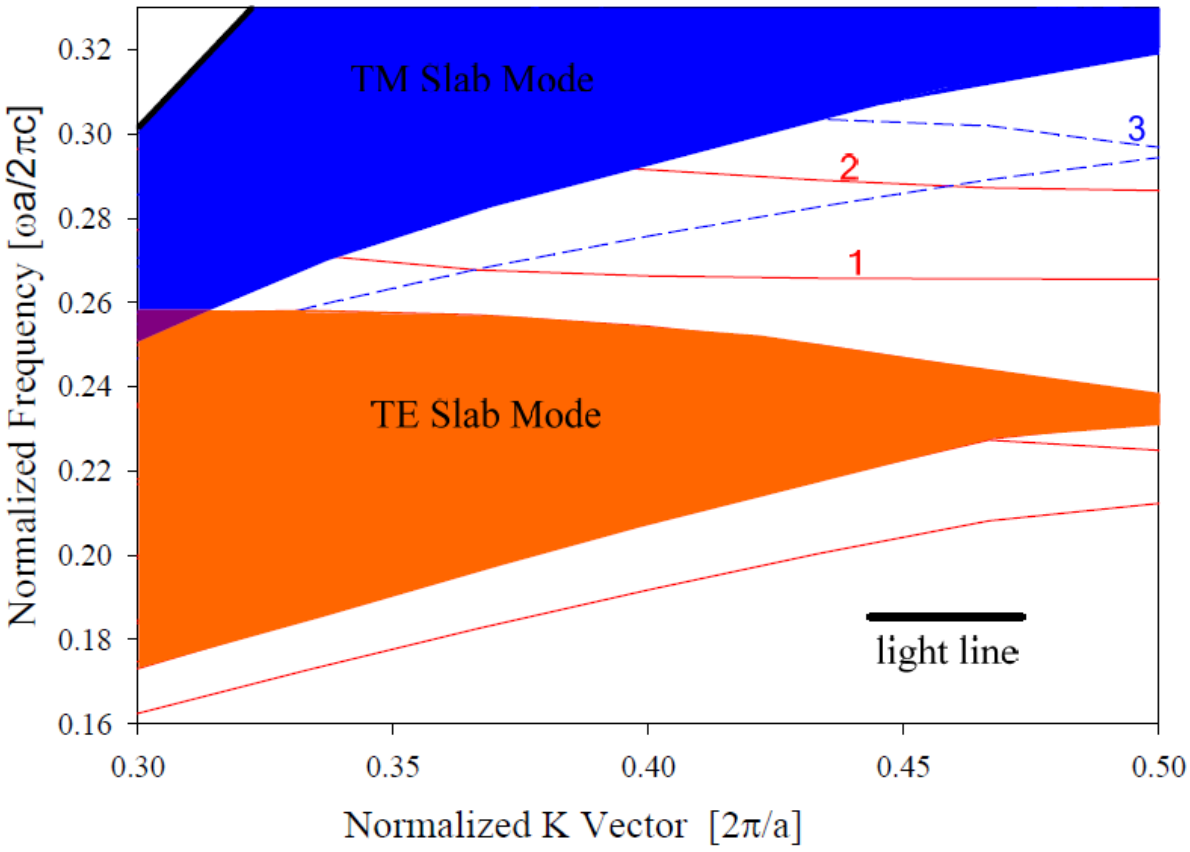

Figure 3.5.2: Projected band structure of photonic waveguide.

3.5.1- TE like guided mode

The guided modes are confined to the line defect. In figure 3.4, the fundamental TE-like guided mode and the second order TE-like guided mode are labeled as 1 and 2. The group velocities of these two guided modes are given by the slope $vg=d\omega/dk$; which approaches zero at the Brillouin zone boundary. This forms the mode edge of the TE-like guided mode, which is very important for creating hetero-junction cavities *[27]*.

Although the electric field of these two TE-like guided modes is vertically even, their horizontal mode distributions are different. The RSOFT FullWave FDTD simulation is used to calculate the electromagnetic field as a function of time and space. The calculated result in Figure 3.5.1(a) to Figure 3.5.1(c) shows the in-plane electric field distribution of the fundamental TE-like mode, and Figure 3.5.1(d) to Figure 3.5.1(f) shows the in-plane electric field distribution of the higher order TE-like mode.

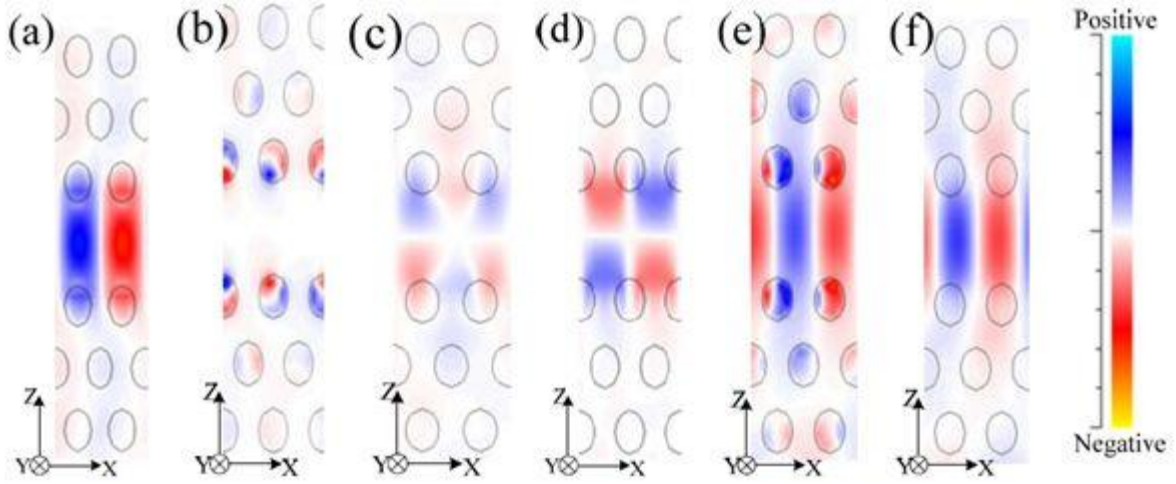

Figure 3.5.3: The field distribution of TE-like guided modes in 2-D PC slab waveguide: (a) Ez of 1st mode.(b) Ey of 1st mode. (c) Ex of 1st mode. (d) Ez of 2nd mode. (e) Ey of 2nd mode. (f) Ex of 2nd mode.

3.5.2: TM-like Guided Modes

Besides the TE-like guided modes, the fundamental TM-like guided mode is also below the light line (labeled as 3 in Figure 3.4). It is a guided mode that is well separated from the continuum of TM-like slab modes in the W1 waveguide. The electric field is vertically odd, and the in-plane distribution of each electric field component is shown in Figure 3.5.2.

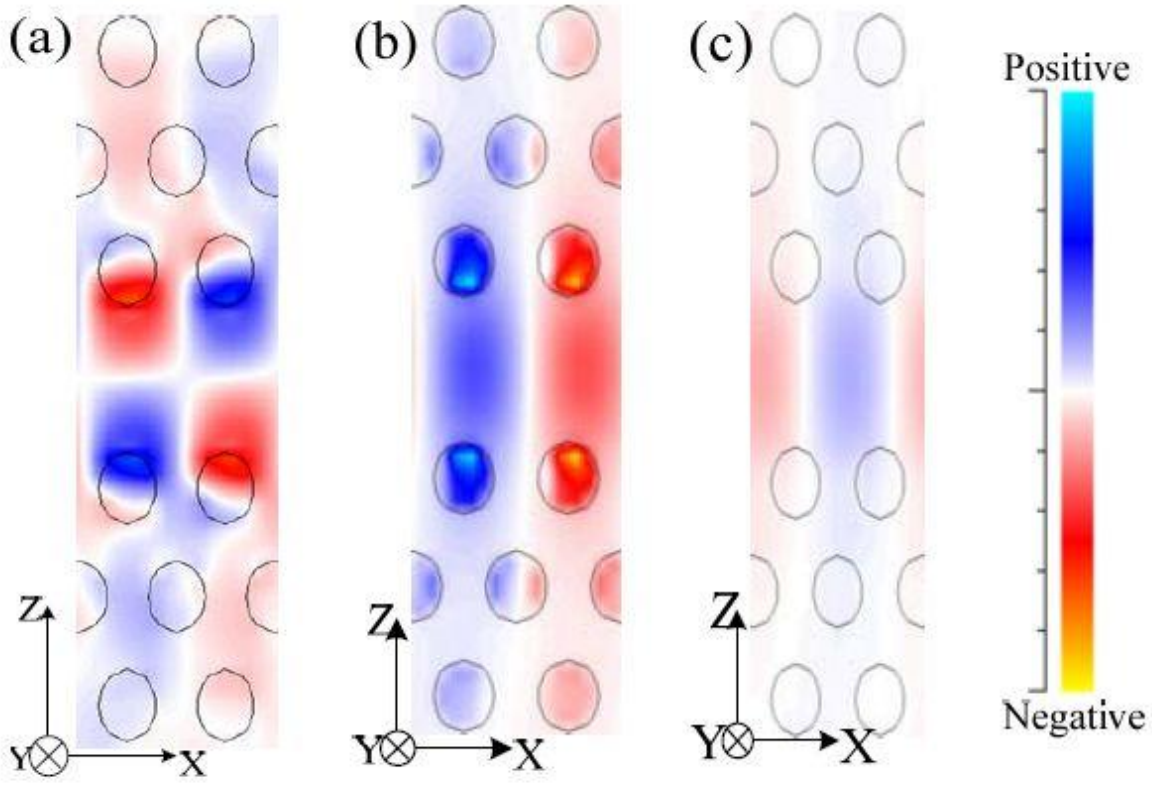

Figure 3.5.4: The field distribution of the 1st TM-like guided mode in 2-D PC slabs waveguide: (a) Ez distribution. (b) Ey distribution. (c) Ex distribution.

Chapter 4

Optimization & Simulation of 2D Photonic Crystal Structures

4.1 Design and Optimization

In this work, an approach is developed to analyze PhC structures. The approach is based on the ***displacement and narrowing*** technique. The motive is to design and optimize the desired photonic crystal waveguides and to optimize the transmission loss. Firstly, a PhC Z-bend consisting of two successive 120° waveguide bends, a Y-bend power splitter waveguide and finally a Mach Zehnder waveguide has been designed. The design has been realized in a gallium arsenide (GaAs) hexagonal photonic crystal waveguide by fabricating air rods/holes. The un-optimized PhC structures display high transmission losses, since the major propagation leakage transpires in the un-optimized bending regions of the PhC structures, thus producing higher transmission losses. The optimization of these designs is done by applying the ***displacement and narrowing*** technique. This technique allows fine-tuning the bending regions of the PhC structures with the aim to curtail transmission leakage throughout the crystal as much as possible and to optimize the transmission loss . The displacement method allows altering positions of certain PhC rods/atoms and the the rods can be moved and placed anywhere within the structure. This breaks the periodicity of the rods of the un-optimized PhC structure. The displacement of these rods is done in the bending regions of the PhC structures. The narrowing technique basically alters the characteristics of the PhC rods/atoms; this means shape or pattern of the PhC rods can be altered by changing its radius, width and other certain parameters. However, the ***displacement and narrowing*** method involves the adjustment of a very important factor, the pitch-ratio (r/a). Radius of the rods is denoted by ‘r’ and the distance from the center of a rod to the center of other rod, which is the lattice constant, is denoted by ‘a’. The default lattice constant is 1. The lattice constant is changed according to the

requirements for the optimization. Same has been done with the radius parameter; the default radius of the rods is 0.2. Similarly, the radius is altered in accordance to the optimization requirements. This is how the pitch-ratio calibrations are made and thus completing the optimization process.

The resulting wave propagation through the optimized waveguides have shown that the modified design areas are enough to yield the wanted improvement in efficiency and the numerical results obtained have shown much optimized transmission losses. The whole design and simulation process including PhC band gap simulation and wave propagation analysis has been done using the software RSOFT.

4.2 Waveguide Design in RSOFT: Drawing in RSOFT CAD

The RSoft CAD is the core program in the RSoft Photonics Suite, and acts as a control program for RSoft's passive device simulation modules BeamPROP, FullWAVE, Band SOLVE, GratingMOD, and Diffract MOD. It is used to define the most important input required by these simulation modules: the material properties and structural geometry of a photonic device. It is needed to typically first design a structure in the CAD interface and then use one or more simulation engines to model various aspects of the device performance. In this work, at first, BandSOLVE module has been used to calculate band gap regions of the desired photonic crystal waveguides. The band gap region gives the required operational wavelengths that can be used to execute FullWave simulation and allow the propagation of light waves transpire throughout the desired waveguides. Secondly, FullWAVE simulation program is used to compute the propagation of light waves through Z bend, Y bend and Mach-Zehnder photonic crystal waveguides.

4.2.1: BandSolve

In principle, BandSOLVE can be applied to find the time-independent modes of any lossless photonic structure. For the most part, however, it is intended to be applied to structures with some degree of periodicity in the refractive index distribution. Indeed, even when applied to non-periodic structures, the calculation is performed by introducing an artificial periodicity. To properly understand the workings of the program and to accurately interpret its results, it is therefore necessary to introduce some basic elements of the theory of (time-independent) electromagnetism in periodic structures.

4.2.2: FullWave

FullWAVE is a simulation package for computing the propagation of light waves in arbitrary waveguide geometries. The simulation is based on the well-known finite-domain time difference (FDTD) technique. This technique is based on direct numerical integration in time of Maxwell's equations using the so-called Yee mesh. FullWAVE employs the perfectly matched layer (PML) boundary conditions for absorbing electromagnetic waves incident on the edges of the computation domain in space. The package allows for both the constant wave and pulsed excitation with a unidirectional or one way source which can be a waveguide mode or a Gaussian beam in the transverse spatial direction. The physical propagation problem requires two key pieces of information:

• The refractive index of distribution.

• The electromagnetic field excitation.

From these, the physics dictates the electromagnetic field as a function of (x,y,z,t) and FullWAVE attempts to calculate this.

4.3- Band Gap Calculation

The degree of a photonic band gap can be considered by its frequency width $\Delta\omega$. However; this is not a very fine calculation. When the crystal is expanded by some factor e, then the equivalent band gap would have a width $\Delta\omega/e$. Here, a gap-midgap ratio is introduced, which is very useful, and is independent of the scale of the crystal *[28]***.** Suppose ω_m is the frequency at the middle of the gap, so the gap-midgap ratio is given by

$$\boldsymbol{\Delta\omega/\omega_m}$$

Where, $\boldsymbol{\Delta\omega}$ is the frequency width of the photonic band gap. It is normally expressed as a percentage. So if the system is scaled up or down, every frequency scale consequently, other than the gap-midgap ratio because it is independent of the scale of the crystal. Therefore, whenever the size or dimensions of a gap is referred, then it basically points to the gap-midgap ratio. The frequency and the wave vector are always plotted in dimensionless units, and are given by:

$(\boldsymbol{\omega a/2\pi c})$ And $(\boldsymbol{ka/2\pi})$

The dimensionless frequency is equal to a/λ, where l is the vacuum wavelength that is given by

$$\boldsymbol{\lambda = 2\pi c/\omega}.$$

4.3.1: Band Structure Calculation Of Photonic Crystal Waveguide Without Defect

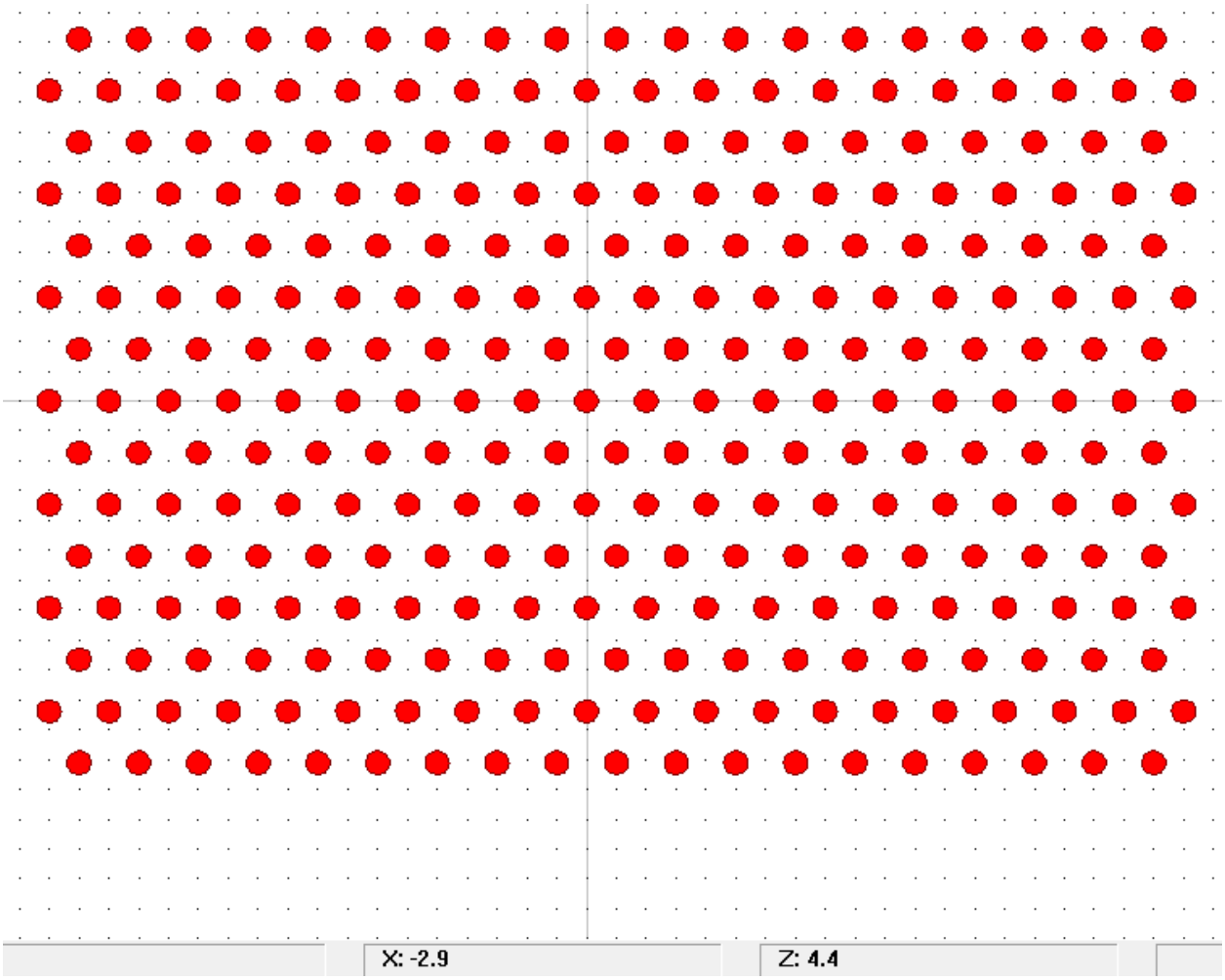

Figure 4.3.1(a): Basic Hexagonal Photonic Crystal Lattice- the red circles are the rods/atoms and the white spaces represent gallium arsenide (GaAs).

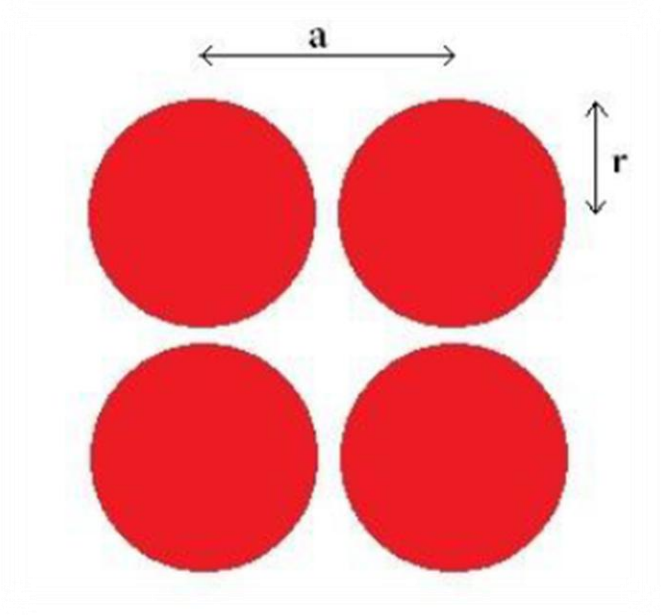

Figure4.3.1(b): Rods in air showing the radius (r) and the lattice constant (a).

Photonic crystals characterizes an interesting feature, that is the photonic band gaps allow certain frequencies of light. With the aid of this unique property, guiding light through the crystal structure can be made possible. This can be attained by introducing defects.

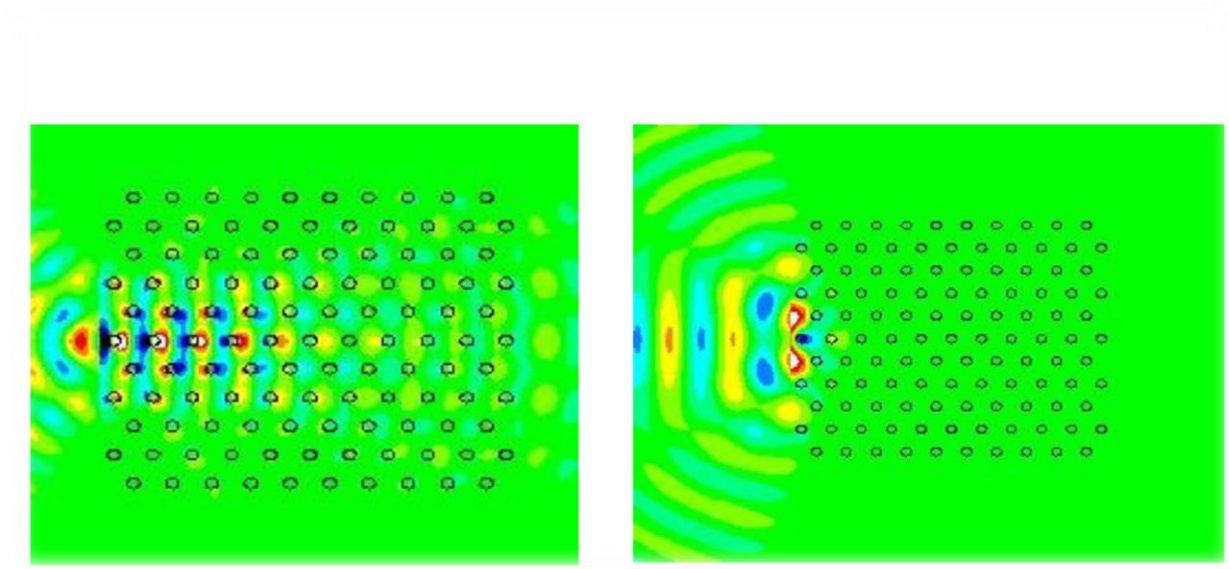

Figure3.3.1(c): (Left) Photonic crystal showing no band gap to a particular wavelength of light and (Right) Photonic crystal showing a band gap to a different wavelength of light.

Photonic crystals (PhCs) are periodic dielectric structures that inhibit propagation of elctromagnetic wave of a certain range of frequencies, therefore introducing a frequency band gap, otherwise popularly known as photonic band gap. To give a clear picture about which wavelengths will show band gap on a particular structure, a dispersion relation diagram is depicted in Figure 4.3.1(d). The dispersion relation diagram shows the dependence of the resonant frequencies on the wave vector of the radiation passing through it.

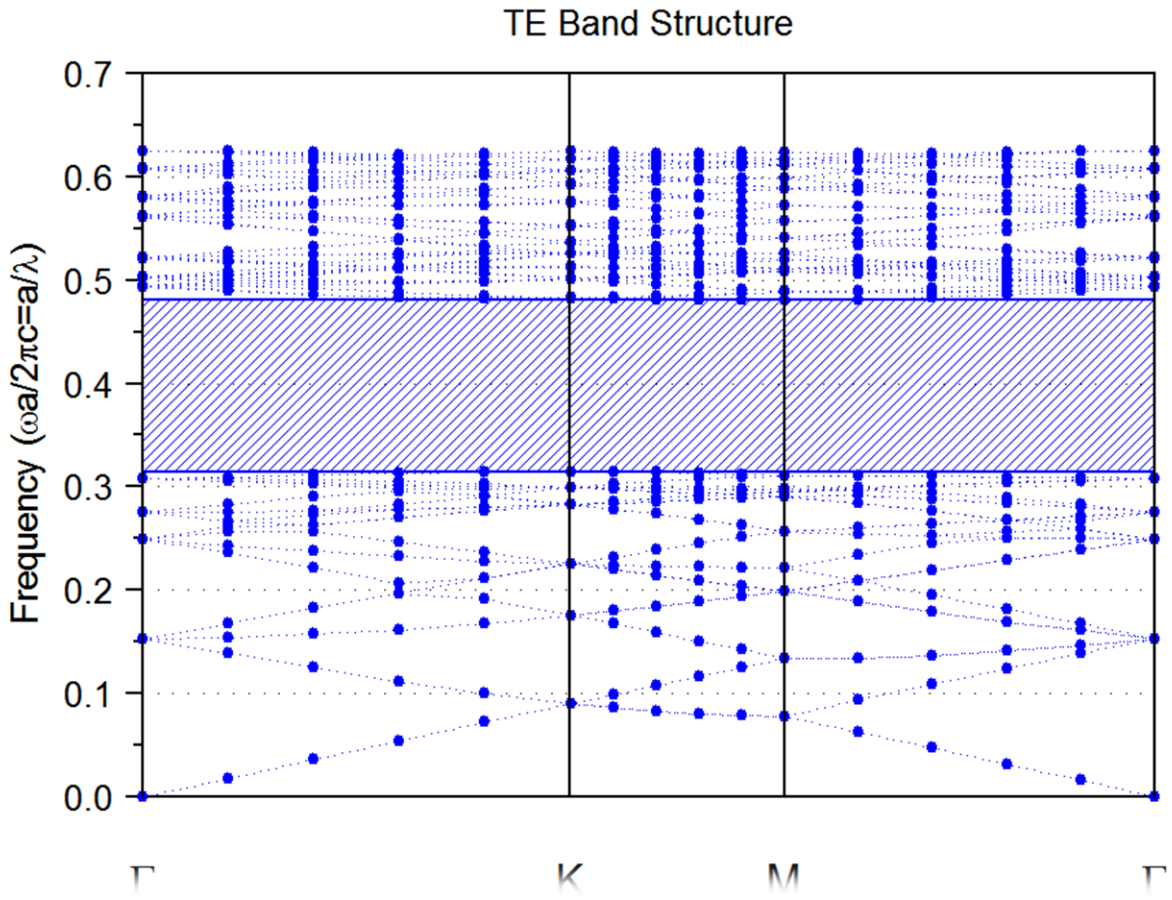

Figure 4.3.1(d): A Dispersion Relation of a Hexagonal Photonic Crystal Lattice computed in Transverse Electric (TE) mode showing the allowed and disallowed modes (band gaps) over the first brillouin zone.

4.4- Simulation of Lattice Defects

In conventional fibers, where light is guided by the total internal reflection, a small bend in the fiber would lead to radiative modes causing a lot of power to leak away. The remarkable effect of photonic band gap can be seen by introducing different shaped defects into the lattice. When light is shone on the lattice, the scattering sites will reflect light back and forth preventing it from propagating forward into the lattice. Consequently, light has no place else to go but to follow the path of the line defect even if it is in the form of a tight bend. This holds great promise for the field of integrated optics that will result in production of miniature low cost optical equipments enabling the optical networking revolution.

4.4.1: Simulating a Z defect in the PhC lattice

In Figure 4.4.1(a) a basic Z, defect is introduced in the hexagonal lattice by removing rods in the desired shape and a Gaussian wave, corresponding to the forbidden mode in the lattice, is launched. The input power is observed to hit the two bending regions of the Z bend waveguide (Figure 4.4.1(b)) and output power is obtained. It is observed that for a given refractive index contrast, and launched wavelength, there exists only one unique value of radius and period for which the corresponding modes are strictly forbidden. The transmission loss has been calculated as the ratio of output transmission to the total input transmission. This transmission loss has been calculated in dB ($10\log\{\frac{Transmitted\ \ Signal\ \ Power}{Incident\ \ Input\ \ Signal\ \ Power}\}$). The corresponding transmission loss for this defect has been illustrated in Figure 4.5(e).

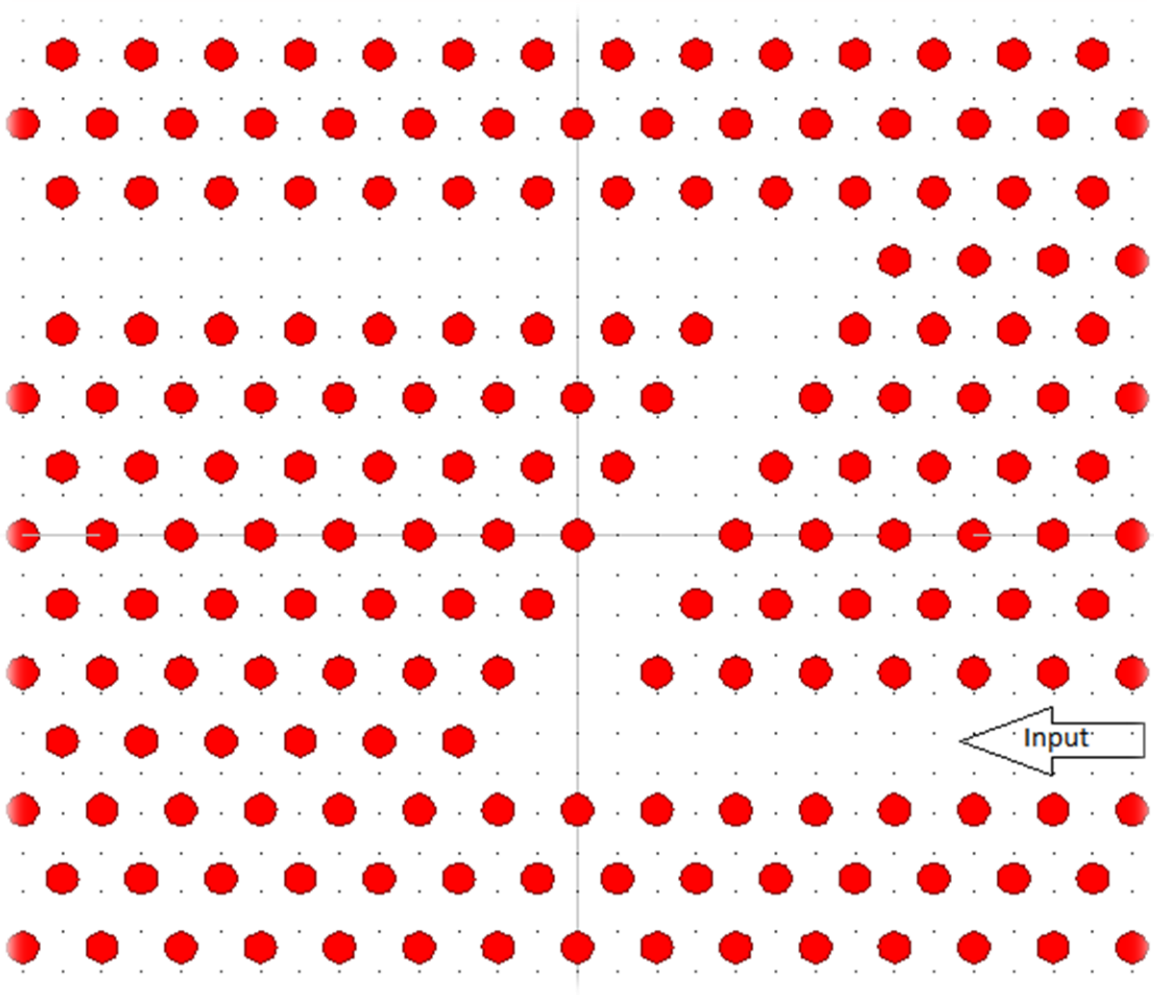

Figure 4.4.1(a): Basic Z defect introduced into the lattice.

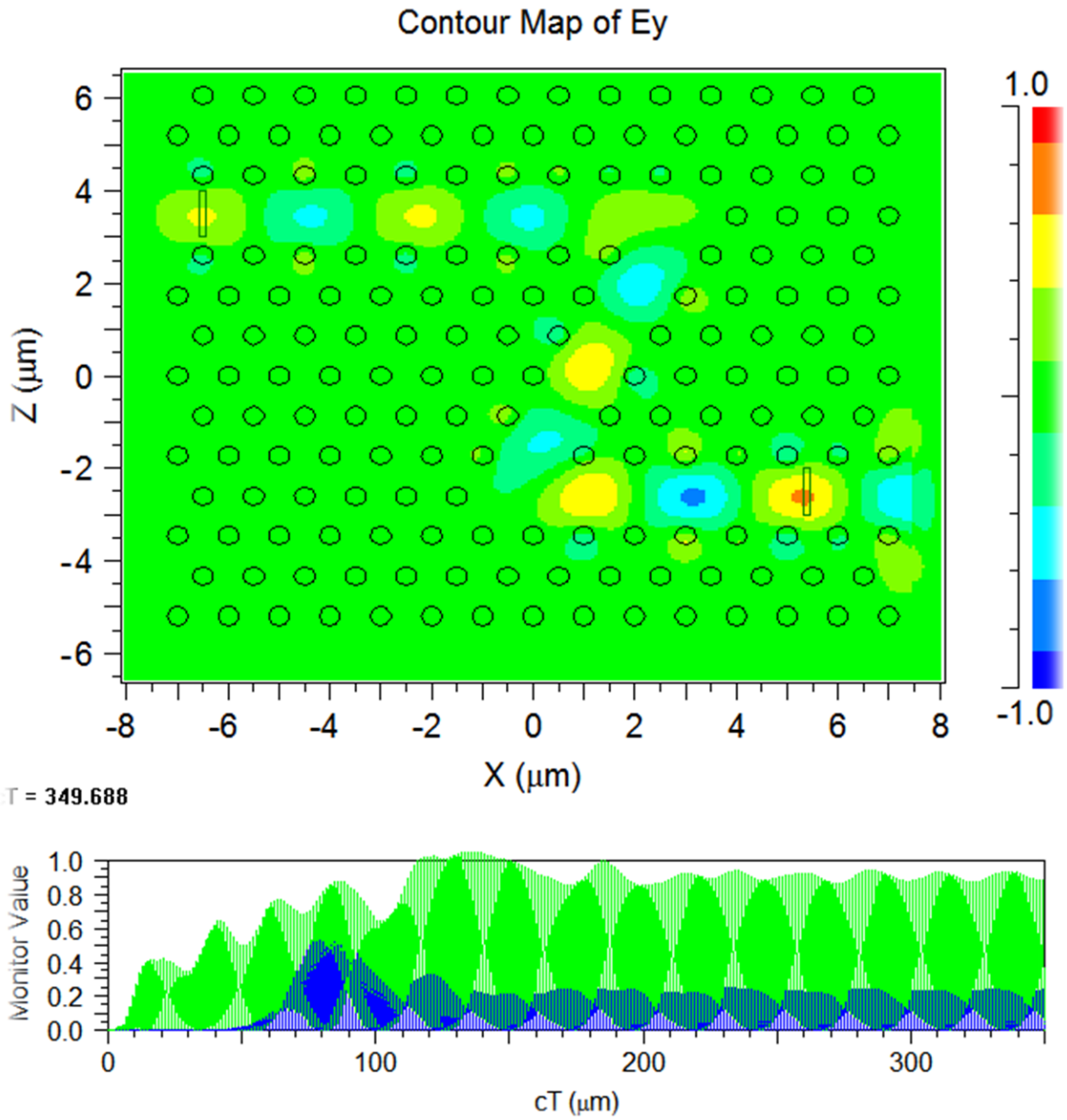

Figure 4.4.1(b): FDTD simulation in basic Z defect.

In Figure 4.4.1(c) Z defect, with the displacement of rods, is introduced in the hexagonal lattice by displacing rods according to the required parameter. The amount of displacement has been done cautiously; the lattice constant of the displaced rods (colored green) in the rectangular boxes has been changed to 0.5µm from the default value 1µm. This means that the distance from the center of the red cell to the center of the green cell inside the rectangular boxes is 0.5µm. Then a FullWAVE simulation, corresponding to the forbidden mode in the lattice, is launched. The input power is observed to hit the two bending regions of the Z bend waveguide Figure 4.4.1(d) and output power is obtained. Transmission loss calculation has been illustrated in Figure 4.5(e).

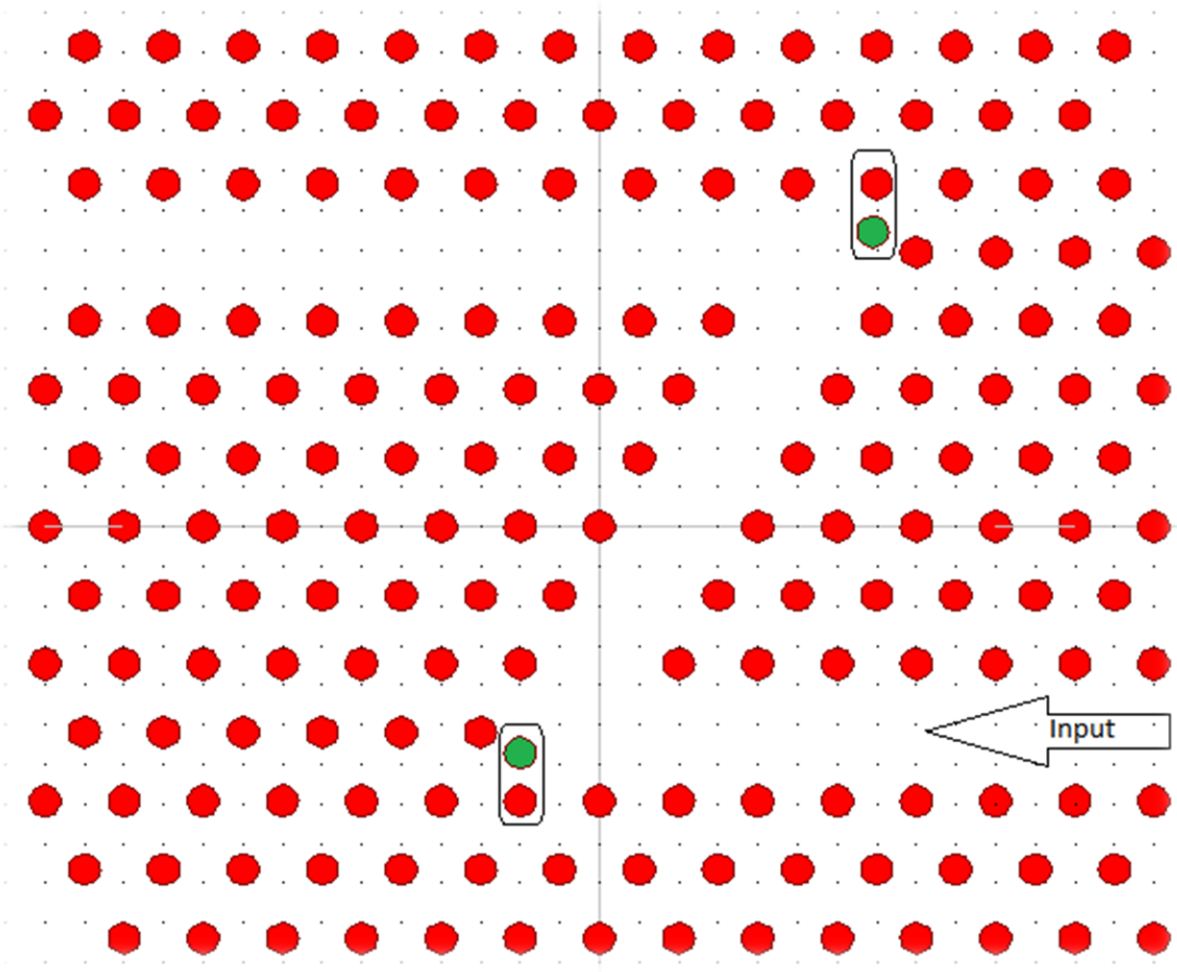

Figure 4.4.1(c): Z defect with the displacement technique introduced into the lattice. The rectangular regions represent the areas where rods have been displaced. The rods that have been displaced are marked green.

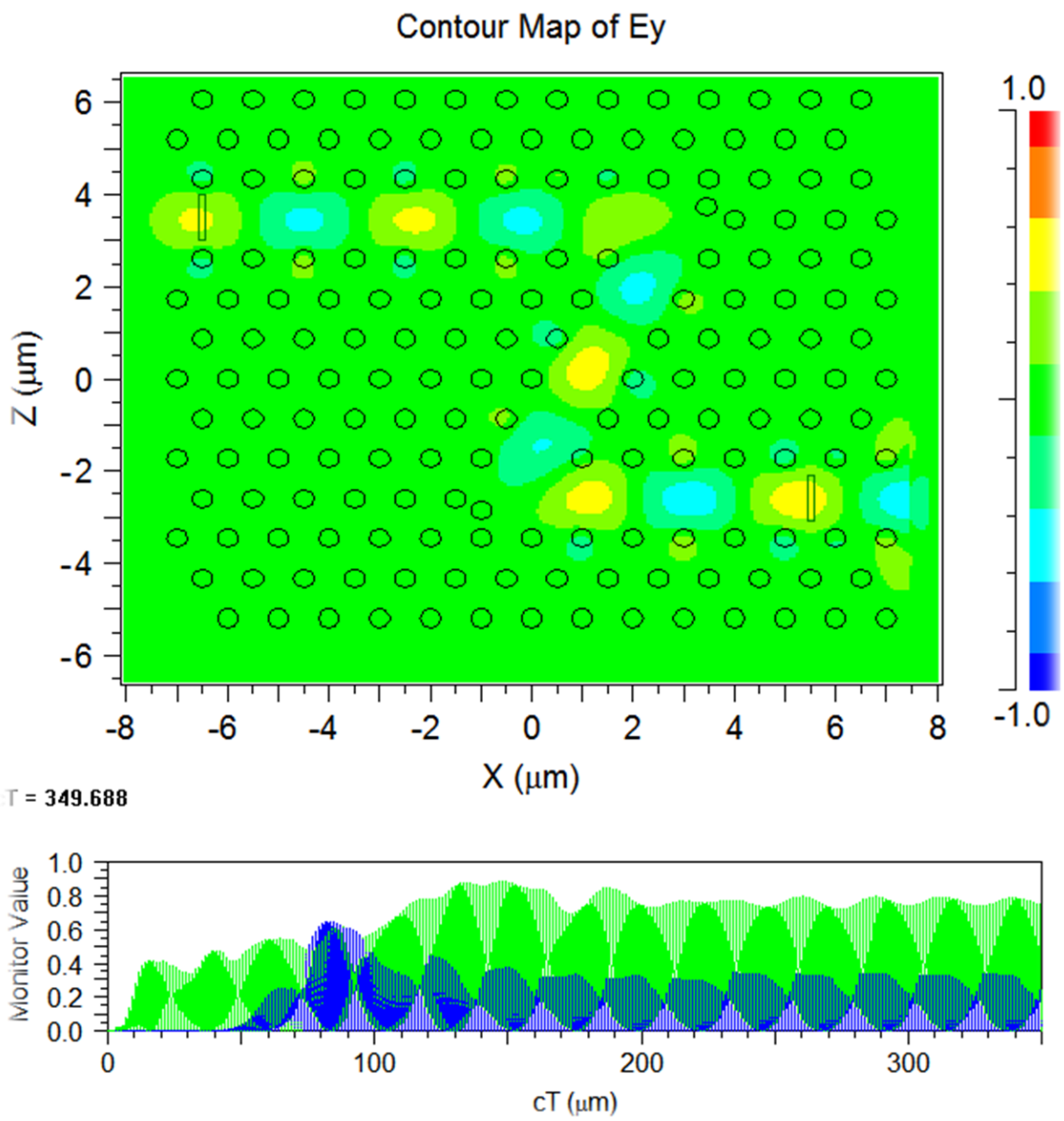

Figure 4.4.1(d): FDTD simulation in Z defect (with displacement technique).

In Figure 4.4.1(e) Z defect, with the narrowing of rods, is introduced in the hexagonal lattice by narrowing rods in the bend regions of the structure. The circled regions in Figure 4.4.1(e) show the narrowing of the rods. The radius of the rods inside the circular regions has been changed to 0.17µm whereas the default radius of the rods is 0.2µm. The simulation program is run, corresponding to the forbidden mode in the lattice. The input power is observed to hit the two bending regions of the Z bend waveguide (Figure 4.4.1(f)) and output power is obtained. The corresponding transmission loss for this modified defect has been illustrated in Figure 4.5(e).

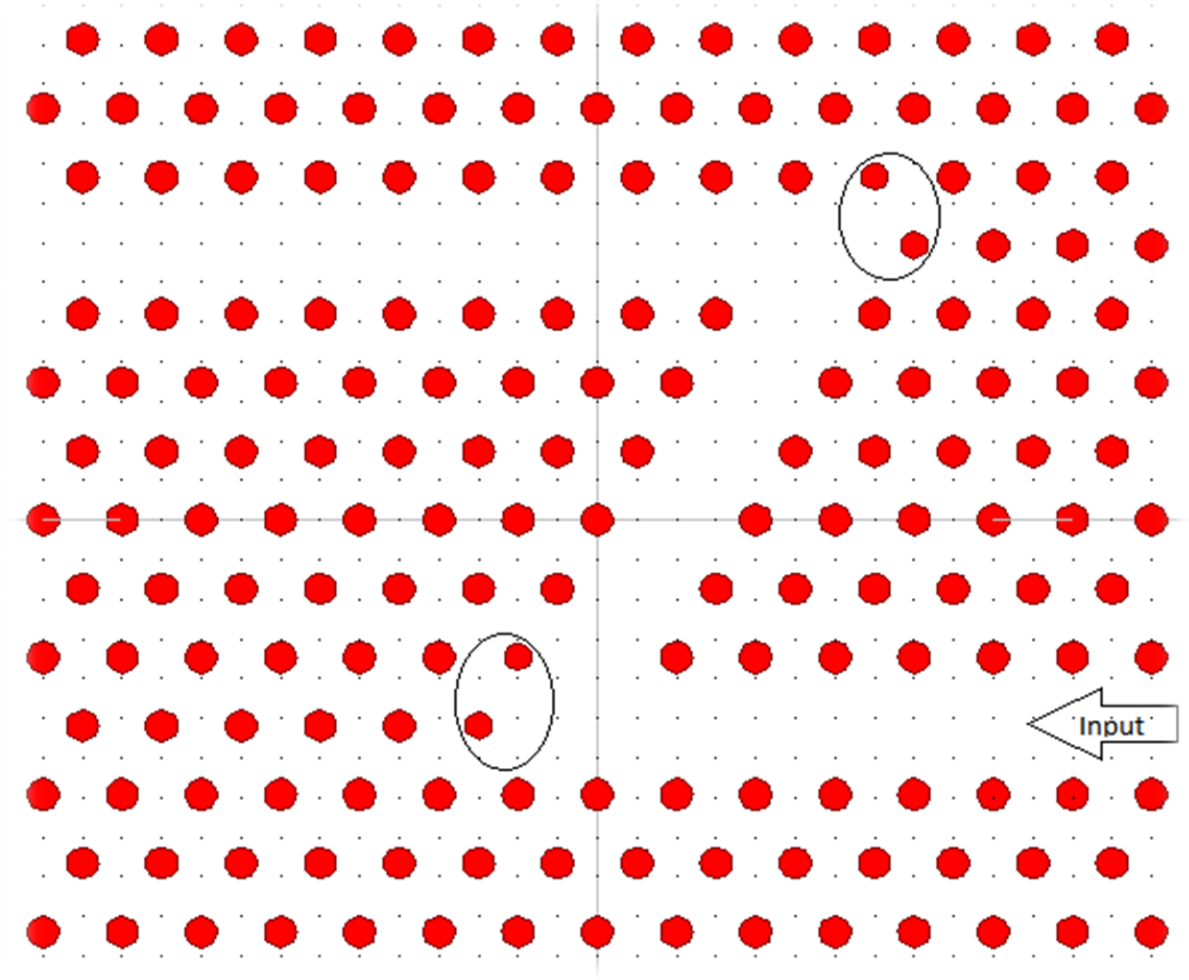

Figure 4.4.1(e): Z defect with the narrowing technique introduced into the lattice. The circled regions represent the areas where rods have been narrowed.

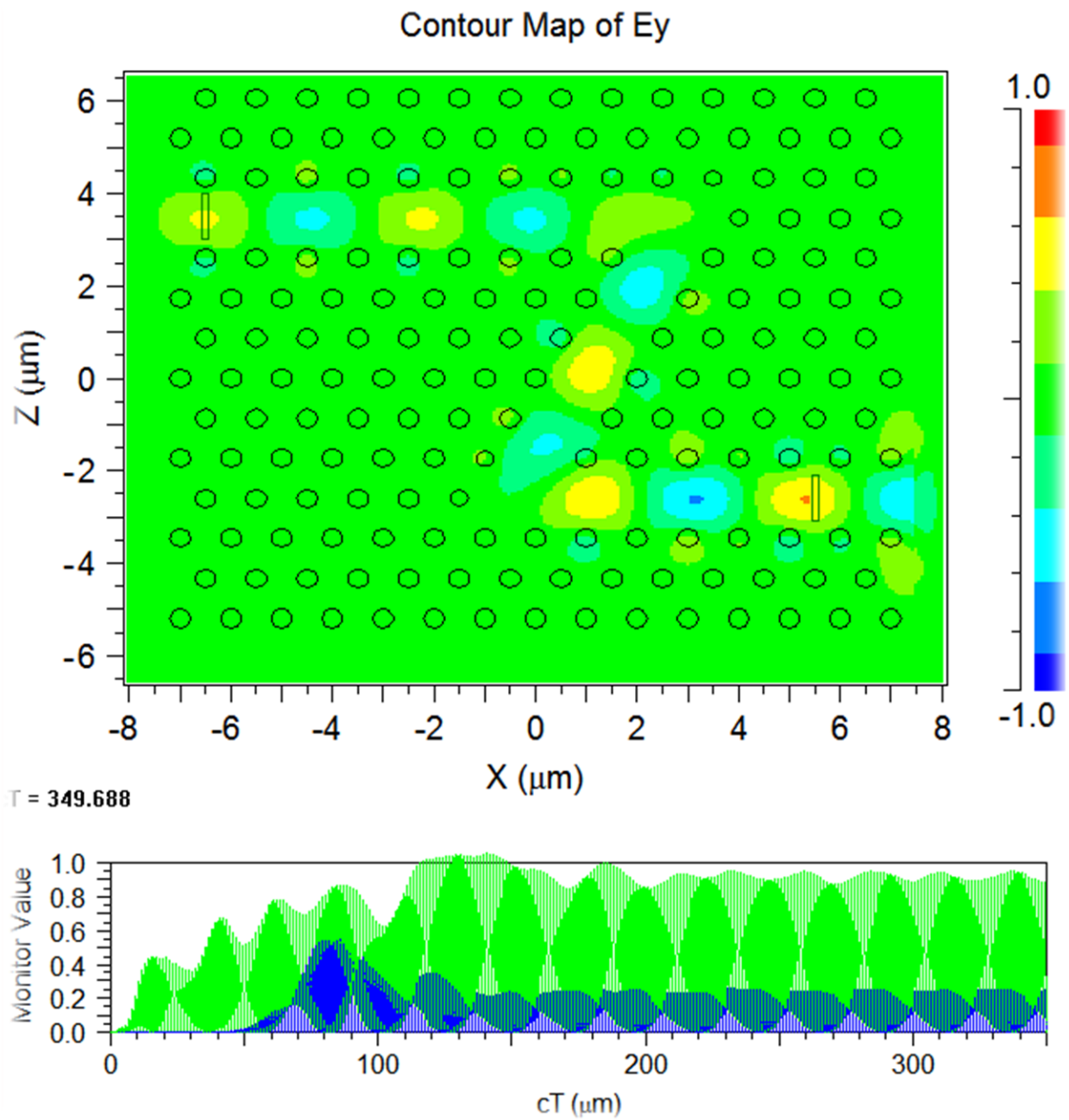

Figure 4.4.1(f): FDTD simulation in Z defect (with narrowing technique).

In Figure 4.4.1(g) Z defect, with the displacement and narrowing of rods altogether (colored in gray inside the rectangular boxes), is introduced in the hexagonal lattice by changing the position of the rods and modifying their width and radius in the bending area of the PhC structure. The radius of the cells marked in gray inside the boxes has been changed to 0.17µm and their lattice constant has been changed to 0.5µm, which means the distance from the center of the gray cell to the center of the red cell inside the box is 0.5µm. After this, a wave is launched, corresponding to the forbidden mode in the lattice. The input power is observed to

hit the two bending regions of the Z bend waveguide (Figure 4.4.1(h)) and output power is obtained. The corresponding transmission loss has been illustrated in Figure 4.5(e).

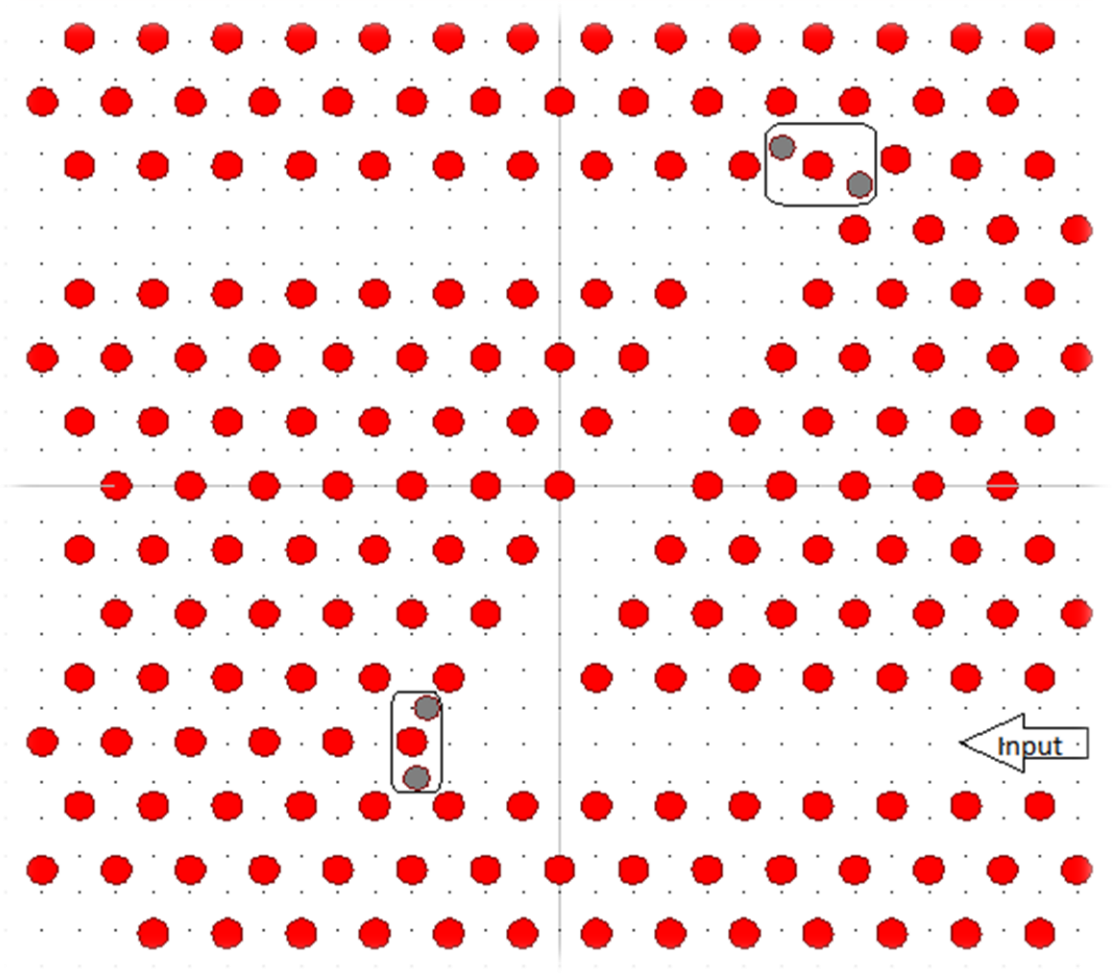

Figure 4.4.1(g): Z defect with the displacement and narrowing technique introduced into the lattice. The rods colored in gray inside the rectangular boxes represent the rods that have been displaced and narrowed.

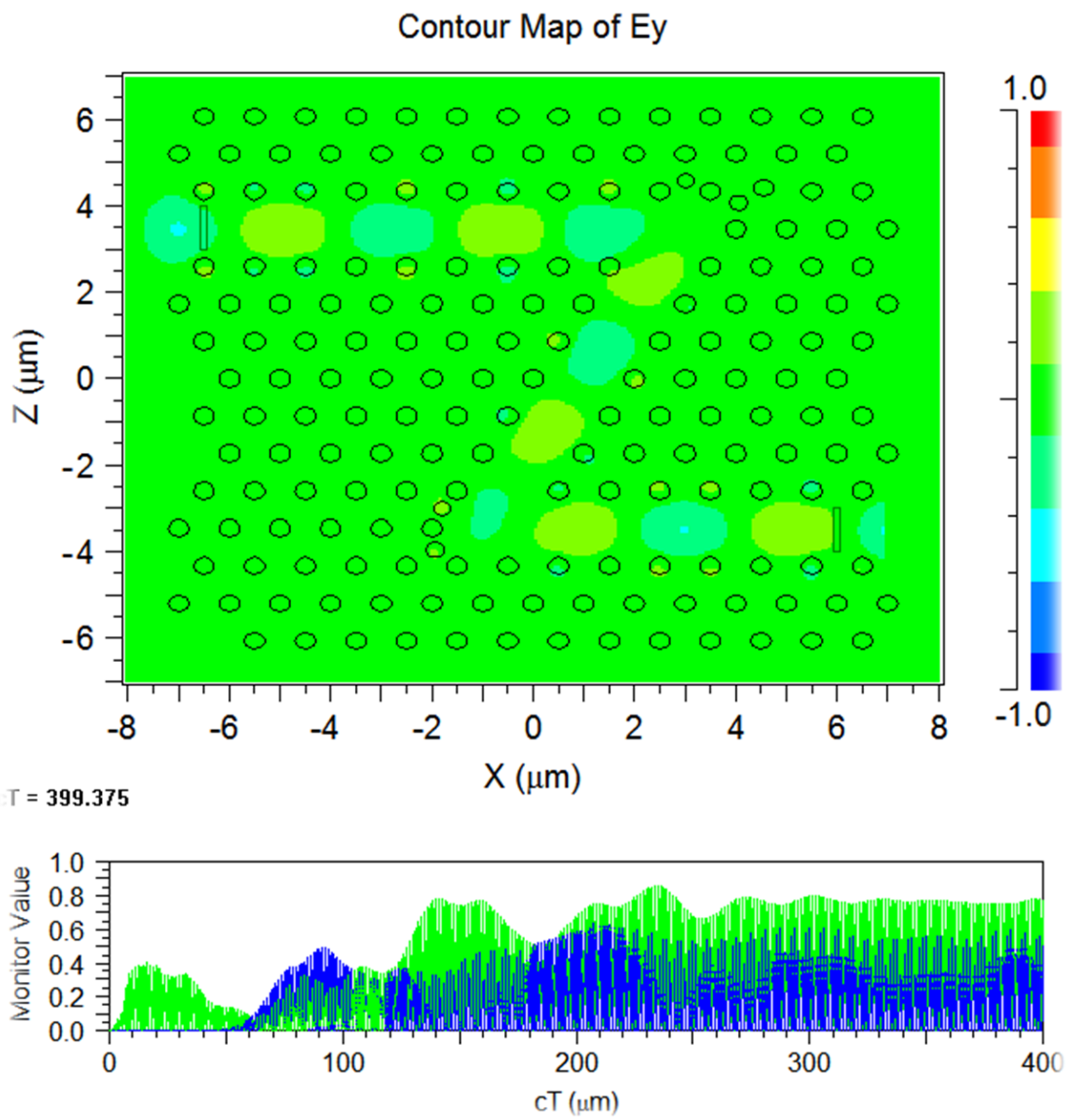

Figure 4.4.1(h): FDTD simulation in Z defect (with displacement and narrowing technique).

4.4.2: Simulating a Y shape defect in the PBG lattice

In Figure 4.4.2(a) a defect in the shape of Y is introduced into the lattice. The defect is simulated (Figure 4.4.2(b)) and the output power is obtained at the output branch. The power is measured at the two ends of the Y and the transmission loss has been calculated in dB. The corresponding transmission loss is illustrated in Figure 4.5(h).

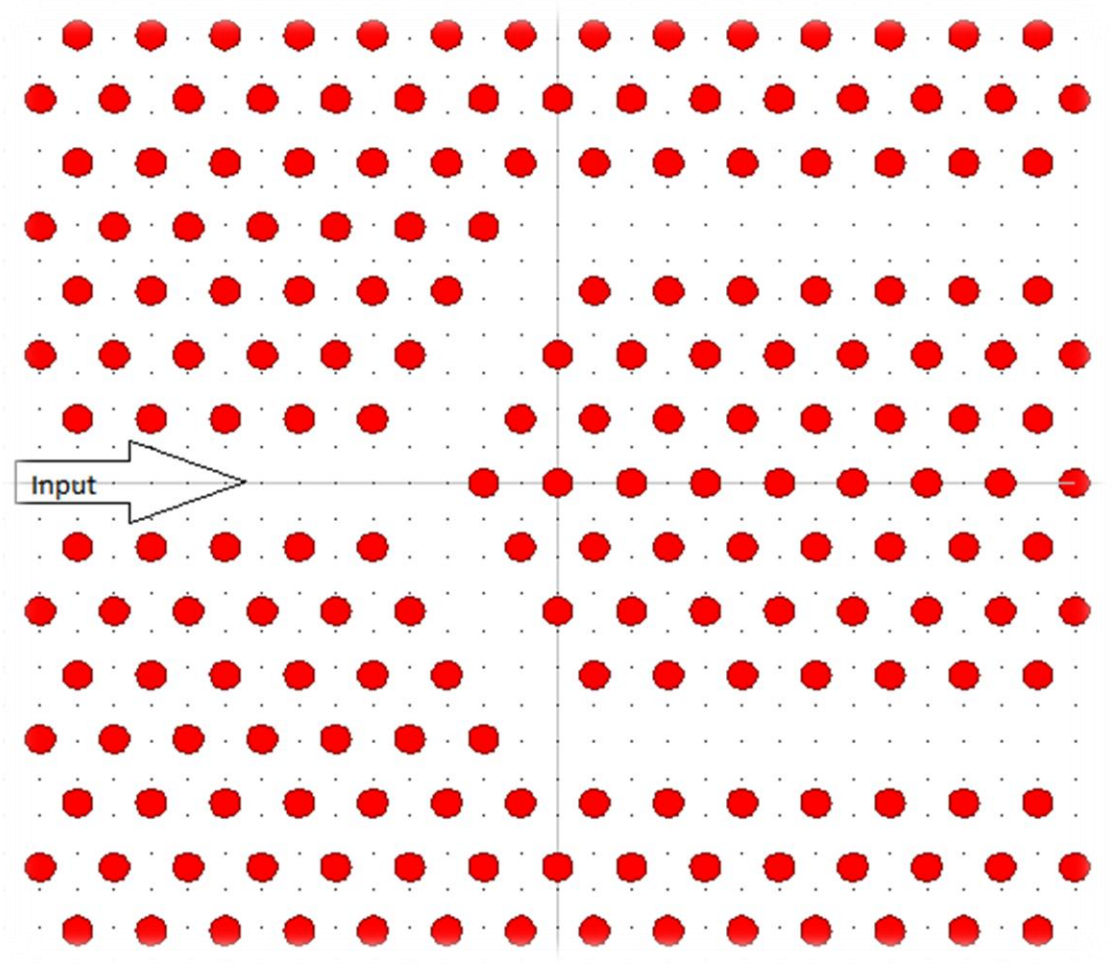

Figure 4.4.2(a): Basic Y defect introduced into the lattice.

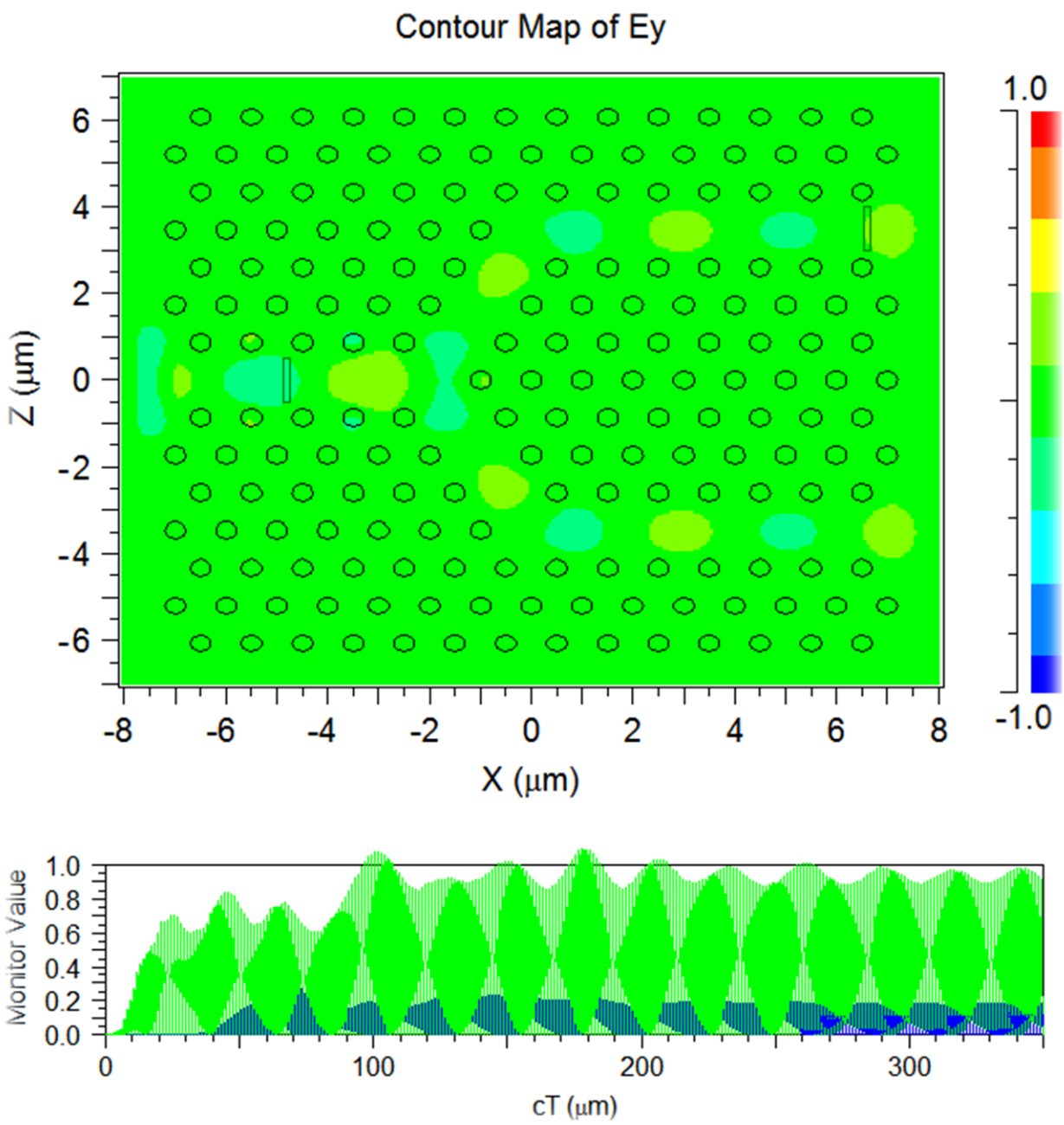

Figure 4.4.2(b): FDTD simulation in Y defect.

In Figure 4.4.2(c) a Y defect, with the displacement and narrowing of the rods (inside the boxes), is introduced into the lattice. The rods that have been displaced and narrowed are marked blue and the rods that have been only narrowed are marked pink inside the rectangular box. For the narrowing purpose, the radius 'r' of the rods inside the boxes is changed to 0.17µm from the default value 0.2µm. For the displacement of the rods, the lattice constant 'a' is changed to 0.5µm from the default value 1µm, which means the distance from the center of a blue cell to the center of a pink cell is 0.5µm. A FullWAVE simulation program for this defect is run (Figure 4.4.2(d)). The corresponding transmission loss has been illustrated in Figure 4.5(h).

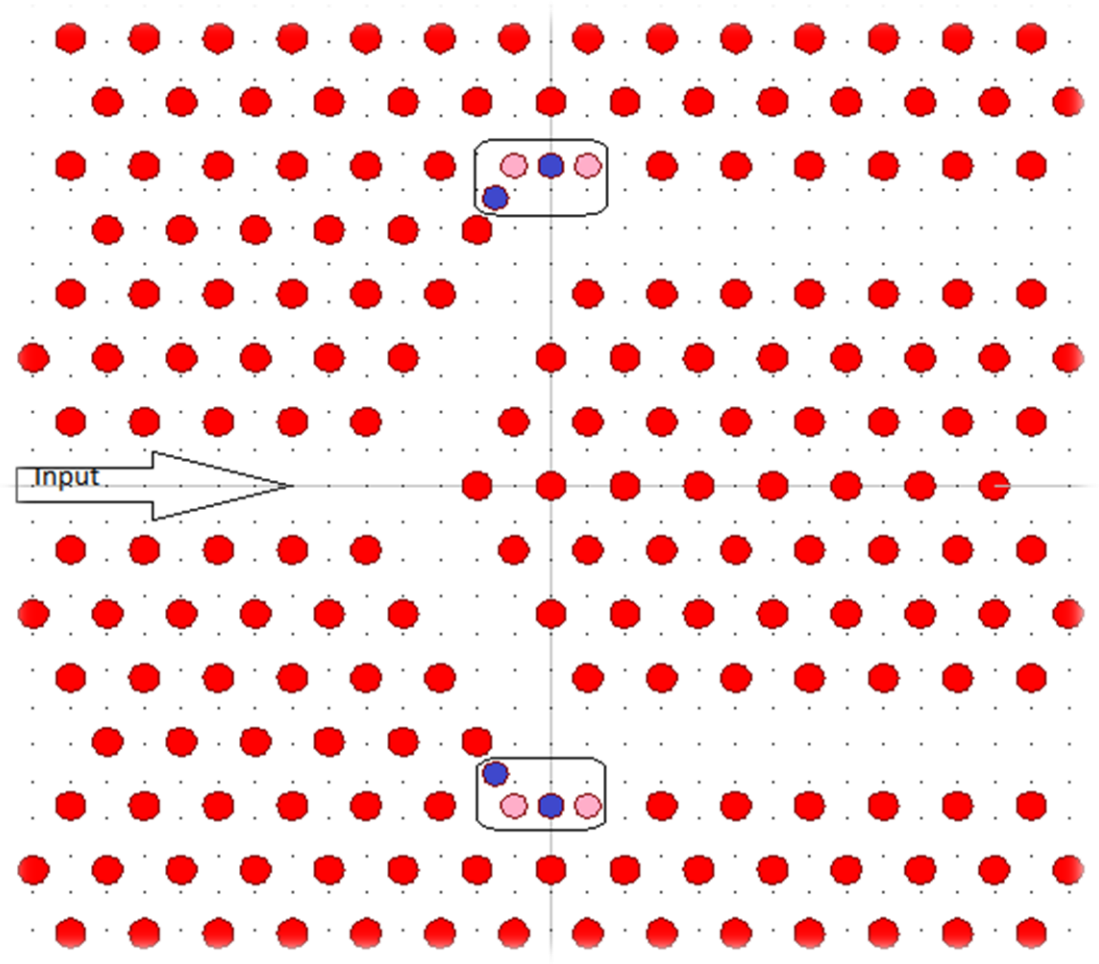

Figure 4.4.2 (c): Y defect with the displacement and narrowing technique introduced into the lattice. The blue cells inside the rectangular boxes represent the rods that have been displaced and narrowed. The pink cells inside the rectangular boxes represent the rods that have been narrowed only.

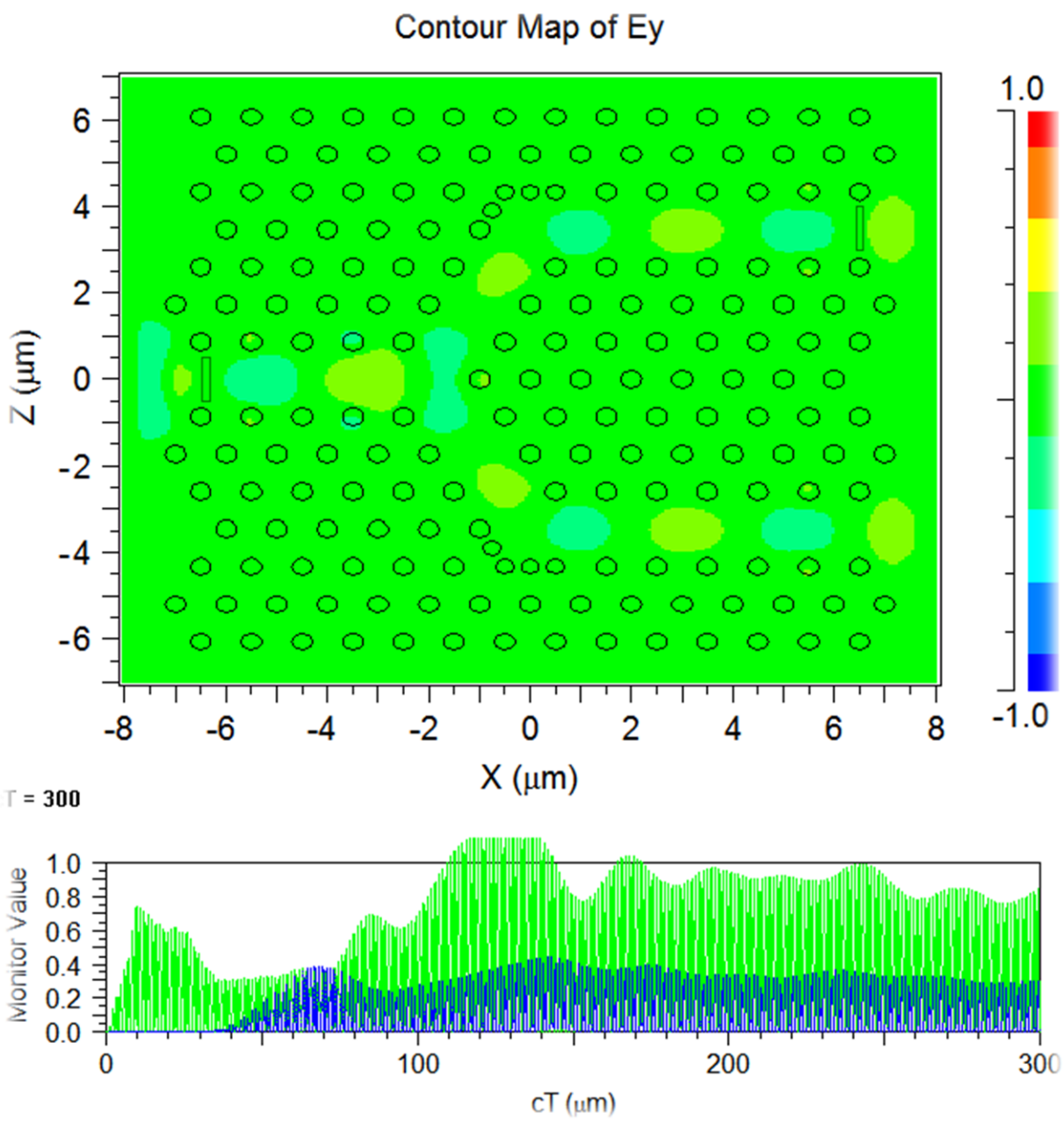

Figure 4.4.2(d): FDTD simulation in Y defect (with displacement and narrowing technique).

4.4.3-Mach-Zehnder Optical Device:

A Mach-Zehnder modulator has an optical splitting element splitting an input optical signal into two optical signals that are conveyed by two optical waveguide arms, and an optical combining element combining the two optical signals into an output optical signal. Two traveling wave electrodes (TWEs) carry an electrical modulation signal to induce a change in phase of these two optical signals, and include a number of pairs of modulation electrodes positioned adjacent to the waveguide arms. At least some of the electrodes in one waveguide arm have a different shape (e.g., length or width) than the electrodes in the other waveguide arm to alter the effectiveness of the electrodes in inducing a phase change in the two optical signals.

Mach-Zehnder modulators (MZMs) are commonly used as transmitters in optical fiber communications systems. One critical parameter in such systems is the amount of dynamic shift in the instantaneous frequency of the optical carrier as it is being modulated with data. Typical data symbol rates are in the range of 2.5 GBd to 100 GBd, while typical optical carrier frequencies are in the range of 190 THz to 210 THz. An induced shift in the instantaneous frequency of the carrier is commonly called frequency chirp, or simply chirp, and can be an amount up to 20 GHz or more, to lower or higher frequencies than the optical center frequency. In many modulated signals, particularly those produced by other means such as directly modulated lasers, and especially those employing a modulation format based on on-off keying (OOK) of the optical power, chirp is an unwanted side effect of the modulation process. Since optical fiber is dispersive, the frequency spectrum of the modulated signal is a dominating factor affecting the quality of the signal as it propagates down a fiber.

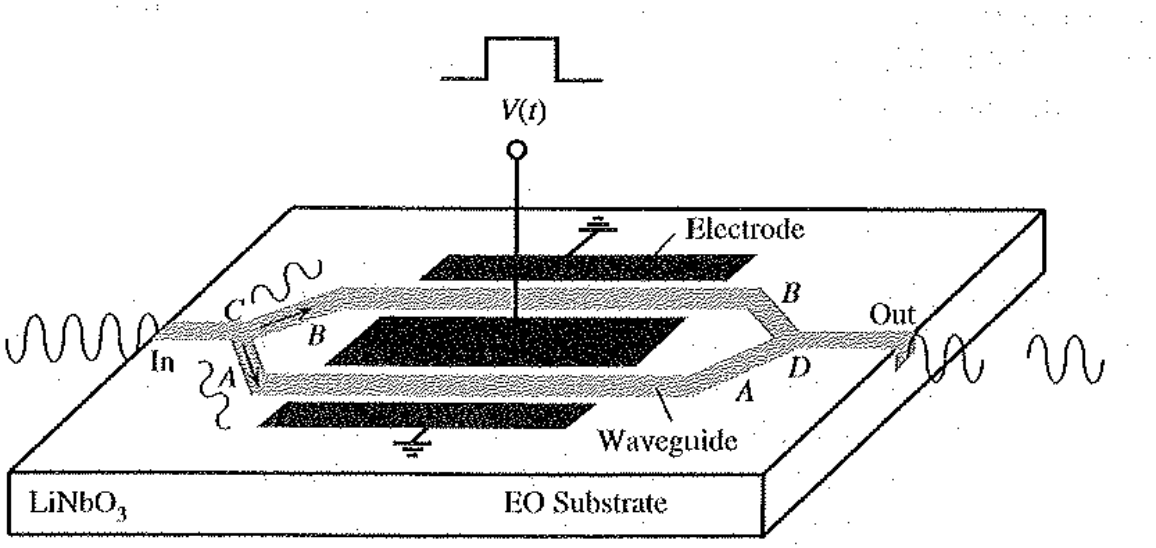

Figure 4.4.3 (a): An integrated Mach Zehnder optical intensity modulator. The input light is

split into two coherent waves A and B, which are phase shifted by a applied voltage and combined again at the output.

Induced phase shift by applied voltage can be converted to amplitude through an interferometer, a device that interferes with two waves of the same frequency but different phase. Consider the structure shown in 4.4.3(a) which has implanted single mode waveguides in LiNbO3, substance in the geometry shown. The waveguide at the input branches out at C to the arms A and B and these arms are later combines at D to constitute the output. The splitting at C and combining at D involve simple Y junction waveguide .The structure acts as an interferometer because the two wave travelling through the arms A and B at the output port D and the output amplitude depends on the phase difference.

4.4.3(a): Simulating a Mach Zehnder defect in the PBG lattice

In Figure 4.4.3(b) a basic Mach Zehnder defect is introduced into the lattice. A Gaussian wave is launched through the input branch (Figure 4.4.3(c)) and the exiting power is obtained at the output branch. The procedure to calculate transmission loss for this defect has been mentioned before. The corresponding transmission loss is illustrated in Figure 4.5(k).

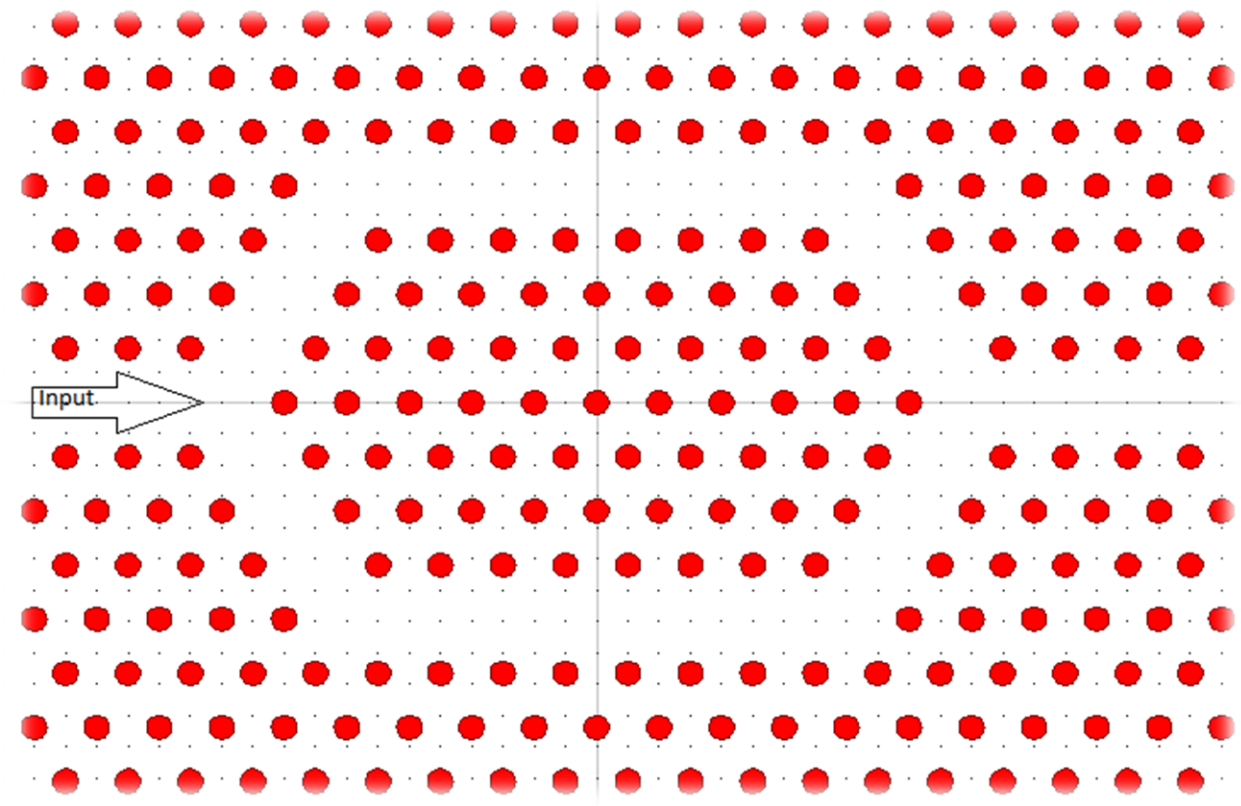

Figure 4.4.3(b): Mach Zehnder defect introduced into the lattice.

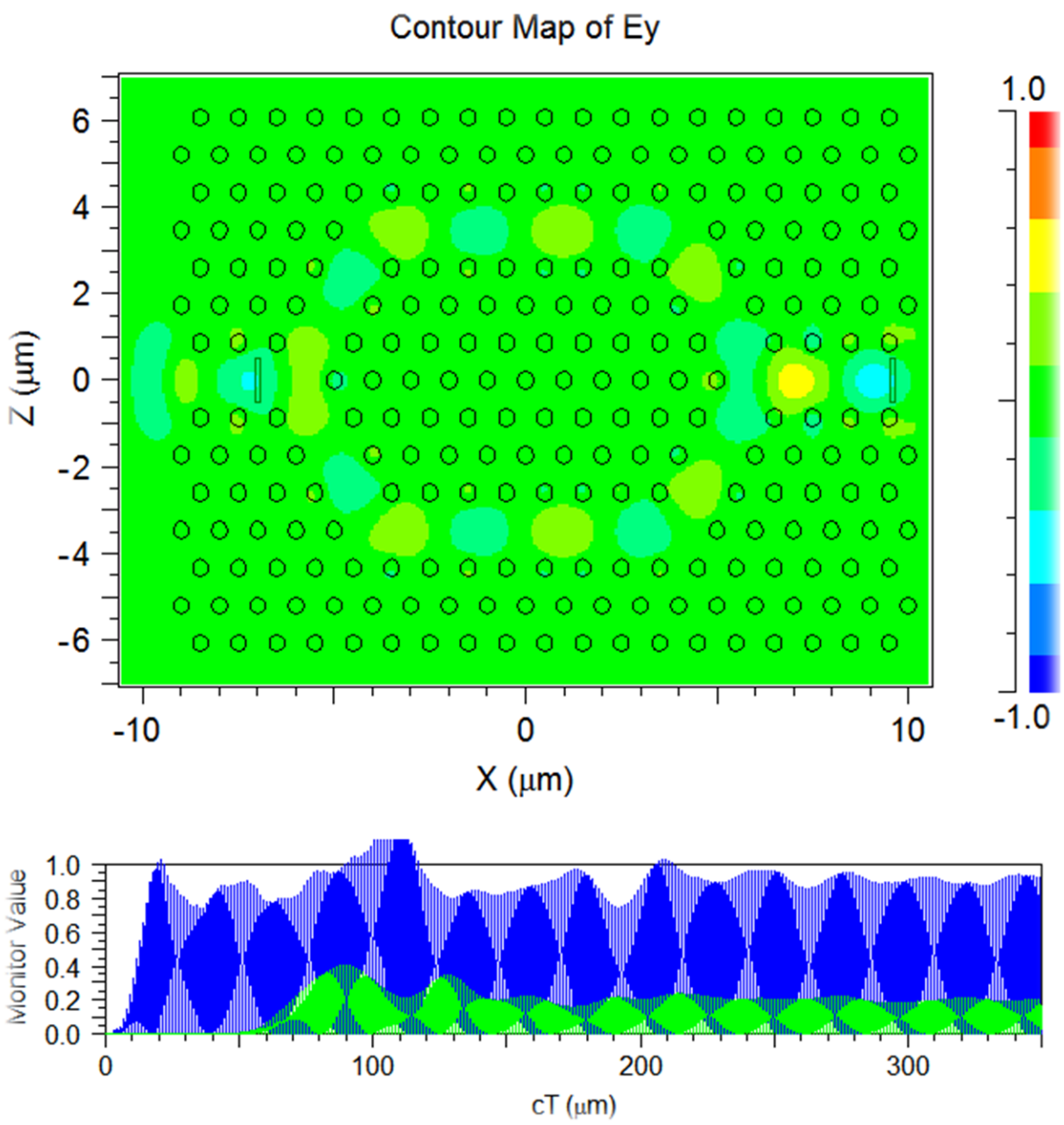

Figure 4.4.3(c): FDTD simulation in Mach Zehnder defect.

In Figure 4.4.3(d) a Mach Zehnder defect, with the displacement and narrowing of rods approach, is introduced into the lattice. The cell which is marked purple has been displaced and narrowed. The radius 'r' of the purple cell has been changed to 0.17µm and its lattice constant

is changed to 0.8µm, which means that the distance from the center of the purple radius to the center of the cell to its right is 0.8µm. The rods in the circular and rectangular area represent the rods that have been only narrowed; their radius 'r' has also been changed to 0.17µm. Simulation program is run for this defect in Figure 4.4.3(e). The corresponding transmission loss has been illustrated in Figure 4.5(k).

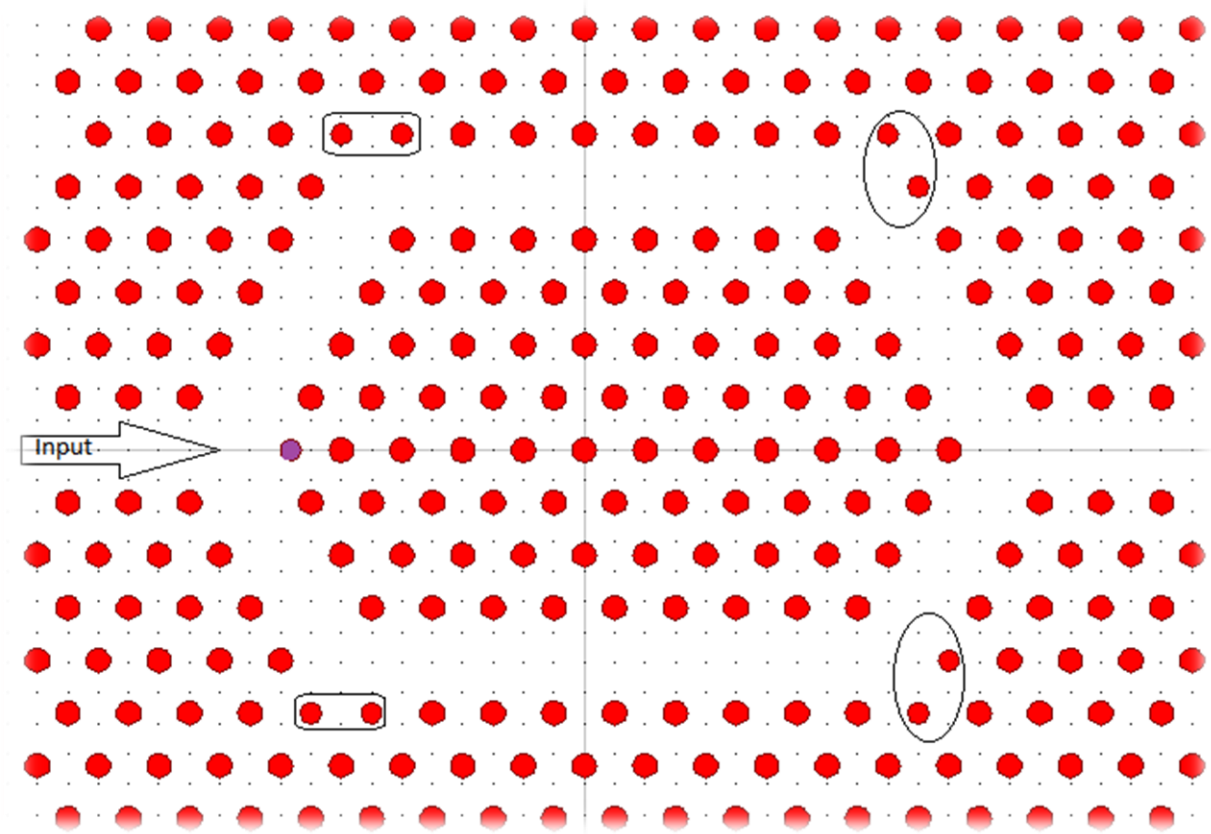

Figure 4.4.3(d) : Mach Zehnder defect with the displacement and narrowing technique introduced into the lattice. The circular and rectangular boxes represent the areas where rods have been narrowed and the purple cell represent the rod that has been displaced and narrowed.

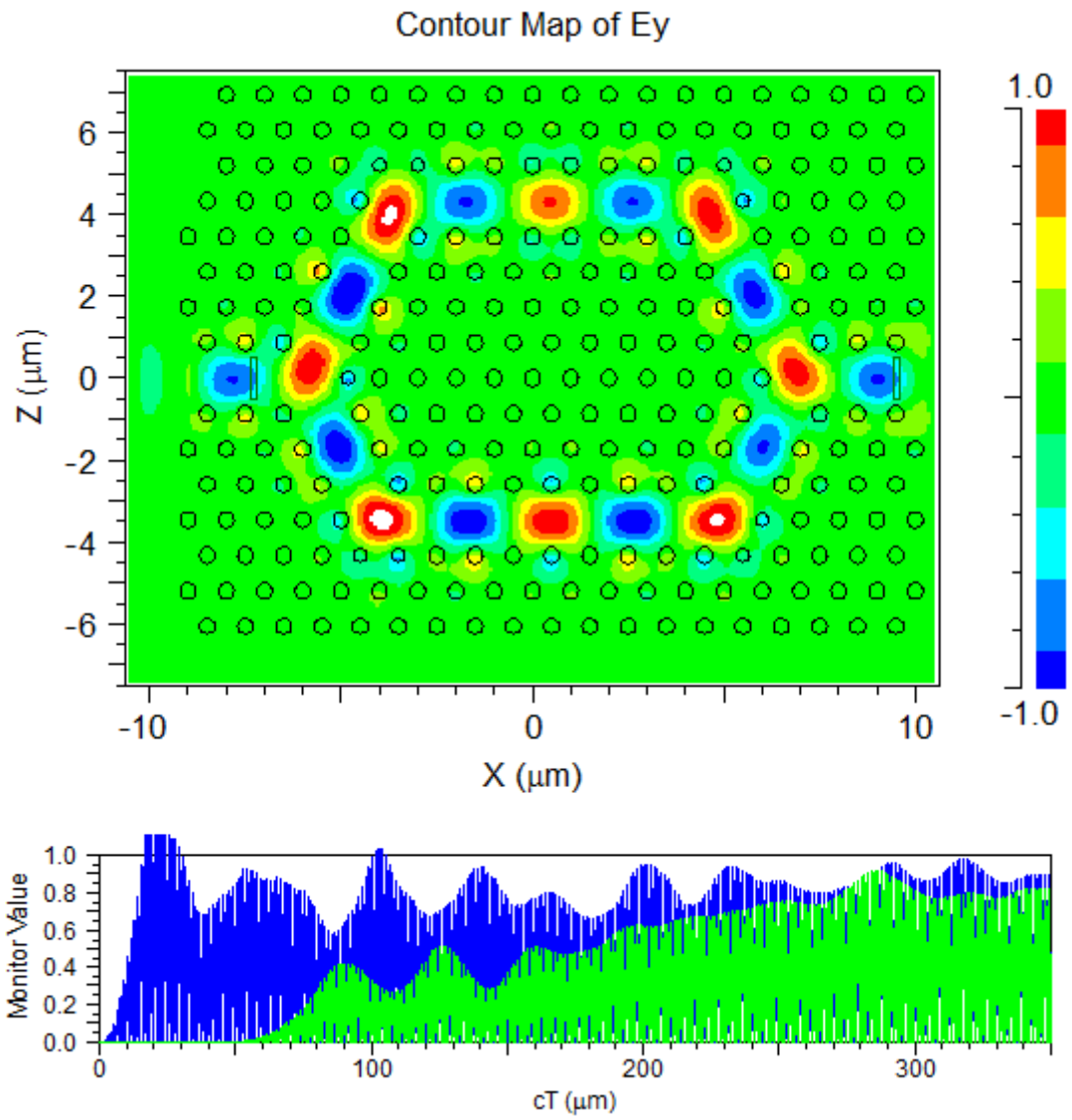

Figure 4.4.3(e): FDTD simulation in Mach Zehnder defect (with the displacement and narrowing technique).

4.5: Transmission Loss Analysis and Results

For all the PhC waveguides, transmission loss has been analyzed with RSOFT using the impulse signal. The dimensionless frequency is equal to a/λ, where 'a' is the lattice constant of the rods and $'\lambda'$ is the wavelength of the propagation. This equation can also be written as λ equal to a/f. The frequency obtained from the dispersion relation of hexagonal PhC lattice in Figure 4.3.1(d) is 0.4μ/m. This means maximum transmission will occur at this particular frequency. Slight increase in transmission loss at other frequencies is noticeable; this is due to the fact that the wave propagation focuses to show higher transmission at 0.4μ/m. Thus by calculation of $\lambda = a/0.4$, the wavelength is found to be 2.5μm. Transmission loss graph has been plotted using the transmission loss equation ($10\log\{\frac{Transmitted\ \ Signal\ \ Power}{Incident\ \ Input\ \ Signal\ \ Power}\}$).

For basic Z defect, the transmission loss analysis is performed using the software algorithm. The transmission loss characteristics have been found and the result has been illustrated in the following figure shown in Figure 4.5(a). From this figure, it has been found that, at 2.5μm wavelength the obtained transmission loss is -6.4085dB.

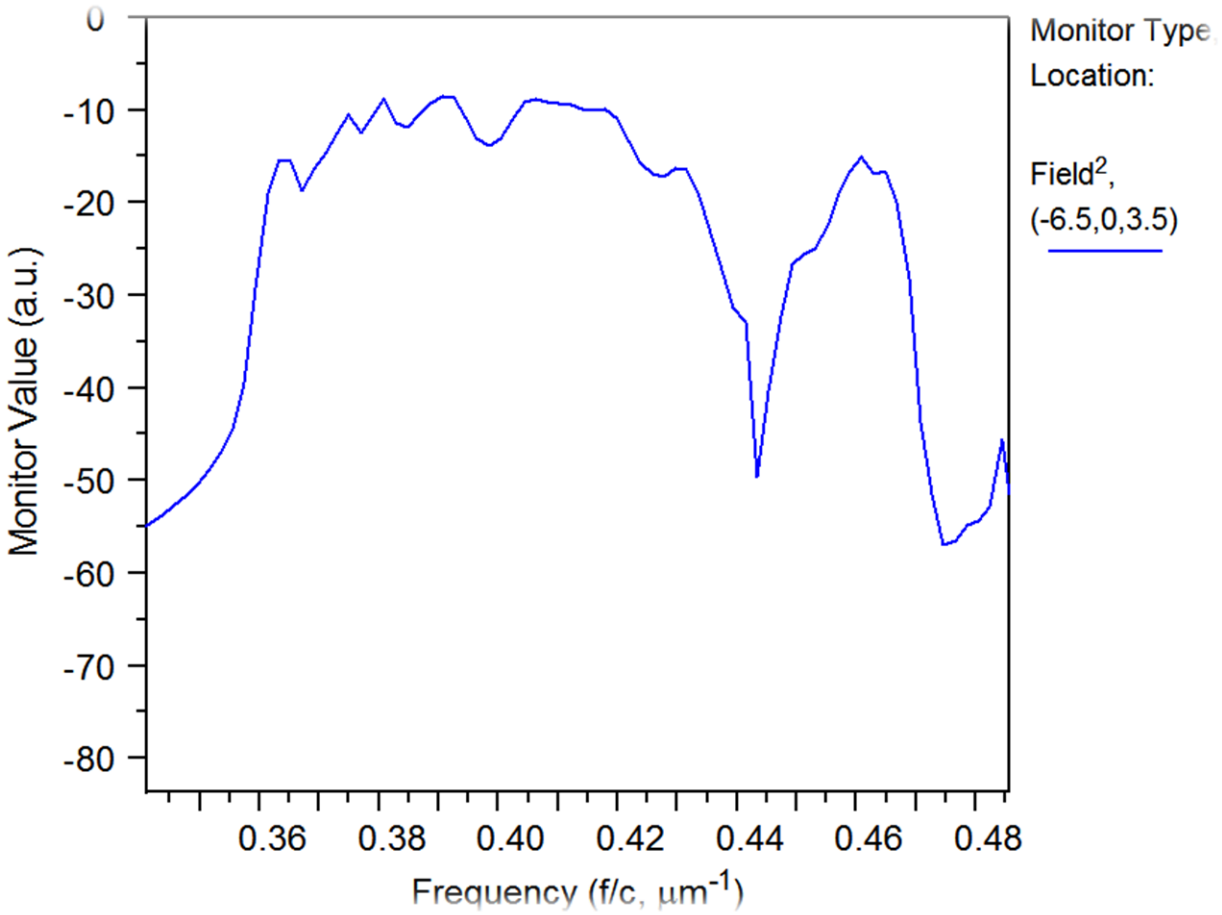

Figure 4.5 (a): Measurement of transmission loss of basic Z defect.

For the optimization of the design, the modification procedures have been consulted at previous discussion. So for the first modification adopting the displacement of the rods of the photonic crystal, transmission loss also has been calculated using the same process mentioned above. The obtained result is shown in Figure 4.5(b). From the figure, it has been found that, at 2.5μm wavelength the obtained transmission loss is -4.3534dB.

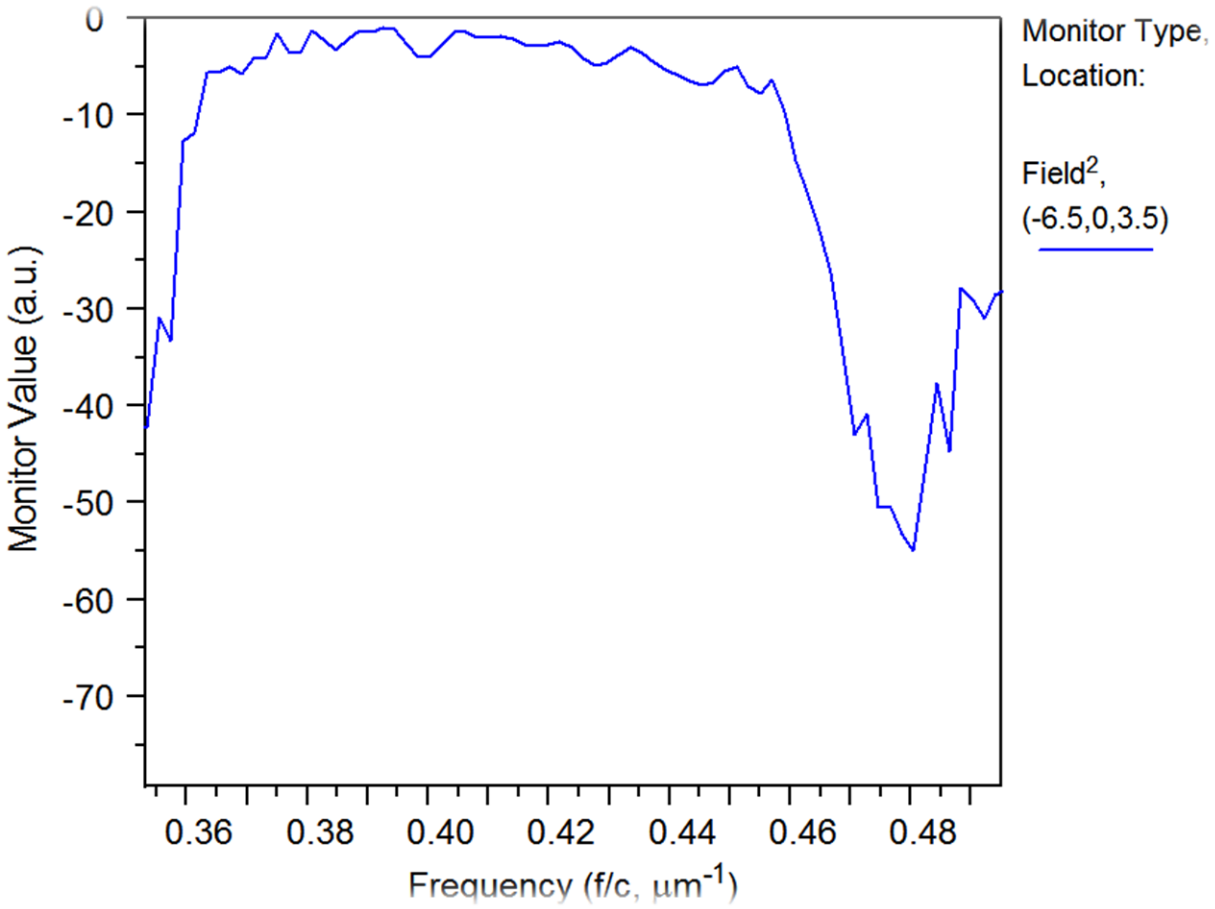

Figure 4.5 (b): Measurement of transmission loss for Z defect with displacement technique.

The second modification adopts the narrowing of the rods of the photonic crystal. Transmission loss has been calculated using the same procedure as mentioned before. The obtained result is shown in Figure 4.5(c). From the figure, it has been found that, at 2.5μm wavelength the obtained transmission loss is -6.0968dB.

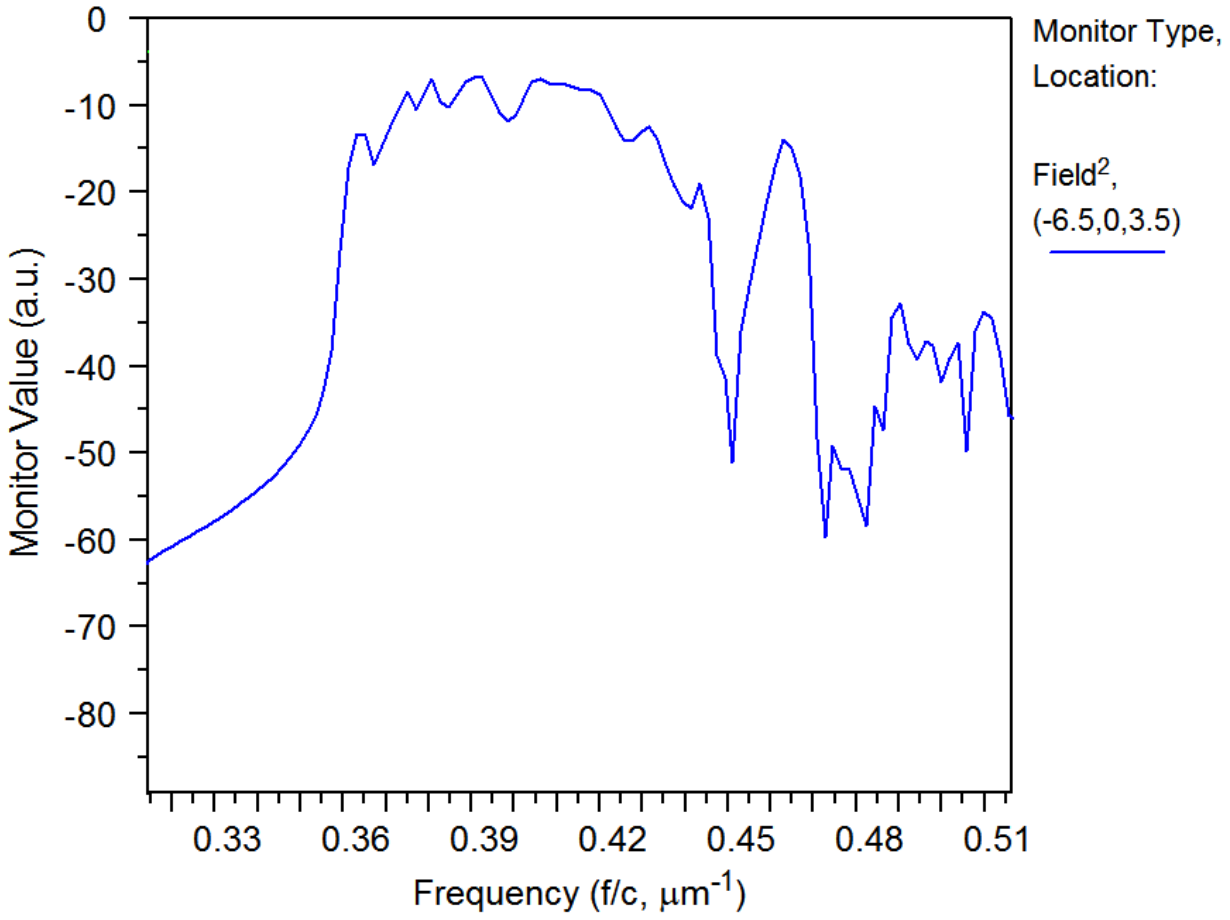

Figure 4.5 (c): Measurement of transmission loss for Z defect with narrowing technique.

The final modification is the displacement and narrowing of the rods of the photonic crystal together. From the modification, the improvement of the transmission loss has been performed with the software adopting the same procedure mentioned at the beginning of this section *4.5*. The modified result of transmission loss of PhC has been given in the figure 4.5(c). From the figure, it has been found that, at 2.5μm wavelength the obtained transmission loss is -

1.5072dB. The obtained transmission loss shows a much improved transmission compared to the previous modifications, thus proving that a much better output can be achieved using the displacement and narrowing technique.

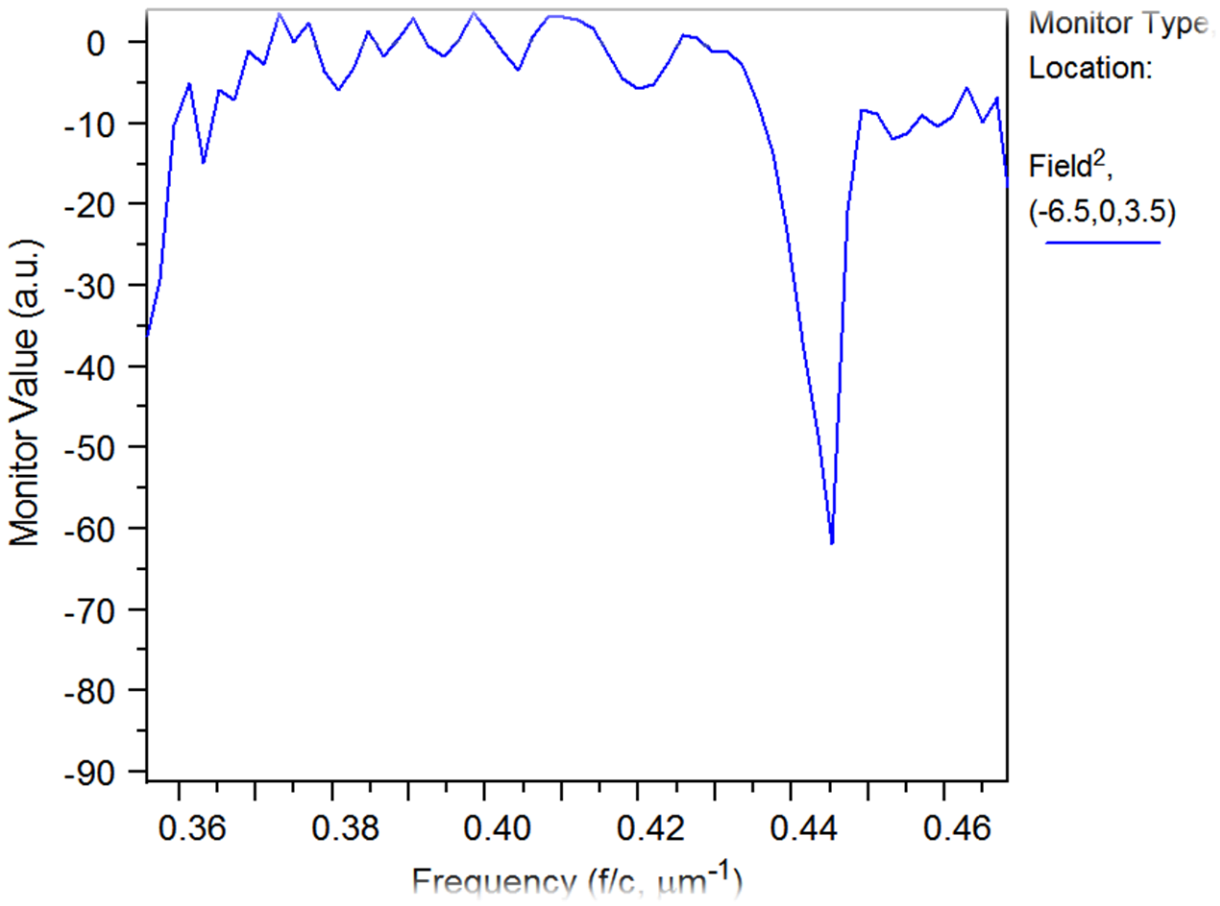

Figure 4.5(d): Measurement of transmission loss for Z defect with displacement and narrowing technique.

Figure 4.5 (e) shows the transmission in dB (defined as $10\log\{\frac{Transmitted\ \ Signal\ \ Power}{Incident\ \ Input\ \ Signal\ \ Power}\}$) for the corresponding Z bend waveguides in a tabular form.

PhC Waveguides	Transmission Loss in dB
Basic Z Defect	-6.4085
Z Defect with Displacement	-4.3534
Z Defect with Narrowing	-6.0968
Z Defect with Displacement and Narrowing	-1.5072

Figure 4.5(e): Table of transmission loss for Z defect.

For Y defect, transmission loss has been analyzed the same way as mentioned at the start of this section. From the analysis using the software algorithm, the transmission loss characteristics have been found and the result has been illustrated in the following figure shown in Figure 4.5(e). From the figure, it has been found that, at 2.5μm wavelength the obtained transmission loss is -7.8969dB.

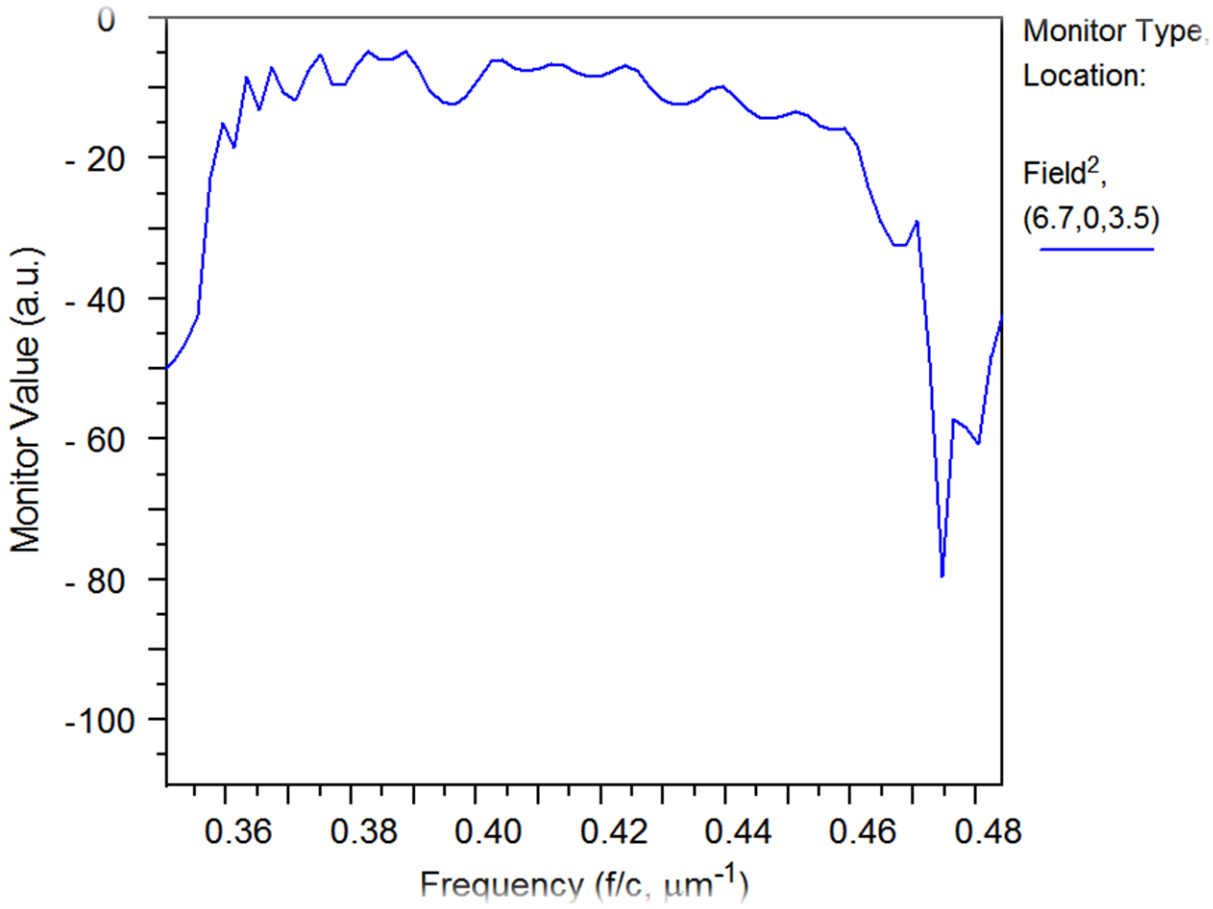

Figure 4.5(f): Measurement of transmission loss for basic Y defect.

The final modification is the displacement and narrowing of the rods of the photonic crystal together. From this modification, the improvement of the transmission loss has been performed with the RSOFT software adopting the same procedure mentioned above. The modified result of transmission loss of PhC has been given in the Figure 4.5(f). From the figure, it has been found that, at 2.5μm wavelength the obtained transmission loss is -6.1502dB. The obtained transmission loss shows better transmission compared to the previous modification, hence proving that a much better output has been achieved -6.1502dB compared to -7.8969dB using the displacement and narrowing technique.

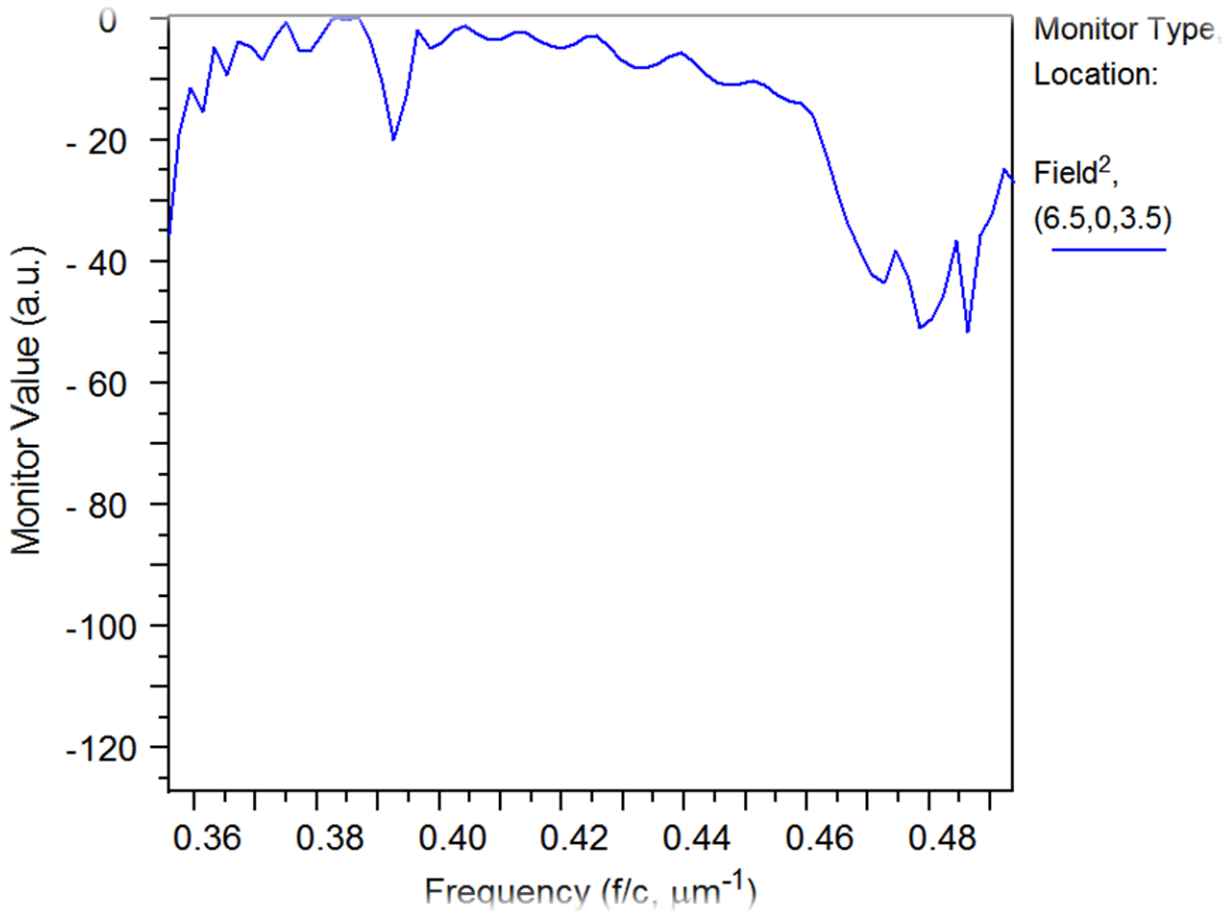

Figure 4.5(g): Measurement of transmission loss for Y defect with displacement and narrowing technique.

Figure 4.5(h) shows the transmission loss in dB for the corresponding Y bend waveguides in a tabular form.

PhC Waveguides	Transmission Loss in dB
Basic Y Defect	-7.8969
Y Defect with Narrowing and Displacement	-6.1502

Figure 4.5(h): Table of transmission loss for Y defect.

For Mach Zehnder defect, from the analysis using the software algorithm, the transmission loss characteristics have been found and the result has been illustrated in the following figure shown in Figure 4.5(h). From the figure, it has been found that, at 2.5µm wavelength the obtained transmission loss is -6.5dB.

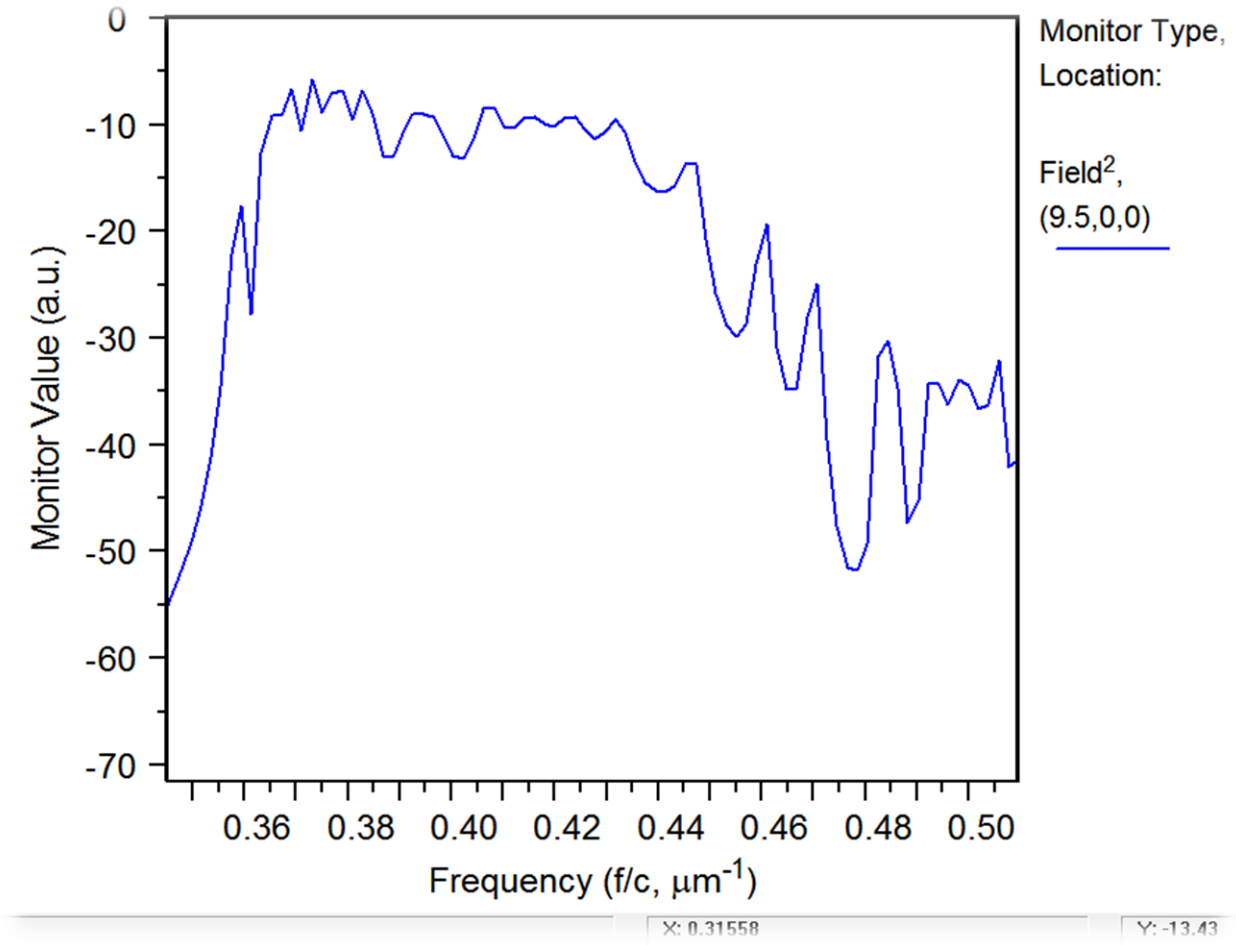

Figure 4.5(i): Measurement of transmission loss for basic Mach Zehnder defect.

The final modification is the narrowing of the rods in the Mach Zehnder photonic crystal waveguide. From this modification, the improvement of the transmission loss has been performed with the RSOFT software adopting the same procedure mentioned above. The optimized result of transmission loss of PhC has been given in the Figure 4.5(i). From the figure, it has been found that, at 2.5µm wavelength the obtained transmission loss is -2.6094dB. The obtained transmission loss shows a much optimized transmission compared to

the basic Mach Zehnder defect, hence proving that a much better output has been achieved -6.5dB compared to -2.6094dB using the narrowing technique.

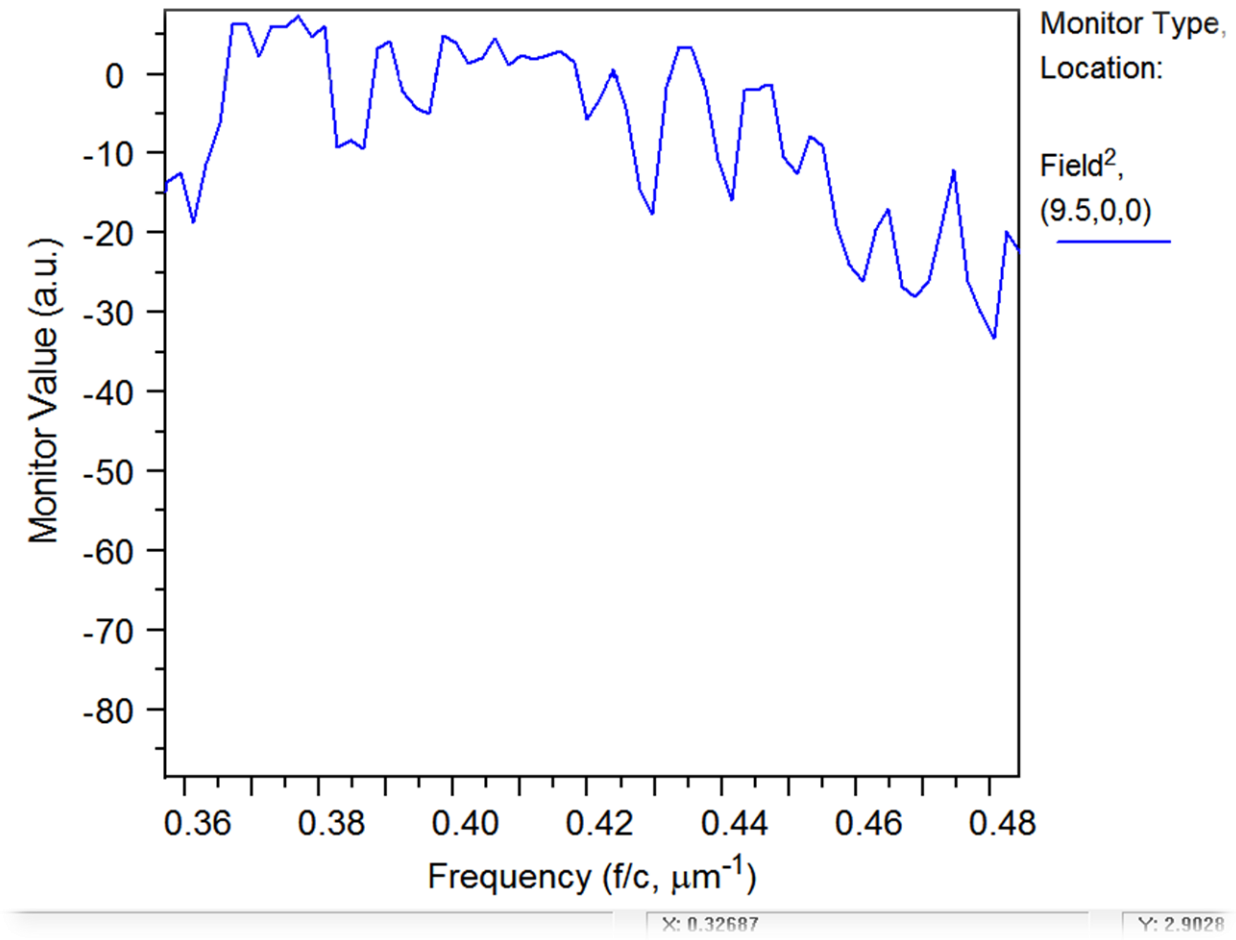

Figure 4.5(j): Measurement of transmission loss for Mach Zehnder defect with narrowing technique.

Figure 4.5(k) shows the transmission loss in dB for the corresponding Mach Zehnder waveguides in a tabular form.

PhC Waveguides	Transmission Loss in dB
Basic Mach Zehnder Defect	-6.5
Mach Zehnder Defect with Dispacement and Narrowing	-2.6094

Figure 4.5(k): Table of transmission loss for Mach Zehnder defect.

Chapter 5

Conclusion

In this work, a number of photonic crystal waveguide structures and devices have been designed and analyzed and identified the basic physical effects that determine their behavior. The main objective of this work was to design Z shape, Y shape and Mach Zehnder photonic crystal waveguides and to optimize the design by introducing displacement and narrowing process. Optimization is justified with the transmission loss calculation. This work has been compared with the previously published work by other researchers on photonic crystals especially on the different bend waveguide. The design and analysis for the transmission loss has been performed using the software RSOFT Cad. In this work, the optical properties of two-dimensional photonic crystals have been theoretically investigated using the methods developed in the framework of the thesis. Simulations that involve introducing Z, Y and Mach Zehnder defects into an otherwise perfect lattice have yielded interesting results.

While Z defects are introduced, the measured transmission spectrum has been normalized to a transmission spectrum for a straight PhC waveguide of the same length. The polarization of the light transmitted through the device containing the Z-bend is analyzed and found to be purely TE polarized. Hence, no significant TE-TM coupling is introduced by the Z-bend. For simple Z-bend photonic crystal waveguide, Z-bend with displacement, Z-bend with narrowing and finally Z-bend with displacement and narrowing has been designed and analyzed separately. The performed results show good agreement with the previously published works *[1]*.

While Y defects are introduced, during analysis it has been observed that light propagation through a basic Y defect without any type of modification exposes more transmission loss compared to Y defect with displaced and narrowed rods. So, a Y defect adopting the displacement and narrowing approach is seen to guide light better than the basic Y defect PhC. To analyze the improvement, transmission loss has been calculated.

The case for Mach Zehnder defect is quite similar to Y, where the splitting and combining of power involve simple Y-junction waveguides. In this case, Mach Zehnder defect adopting the displacement and narrowing method has shown better output, a much more optimized transmission loss compared to the normal Mach Zehnder defect.

In almost all the cases, the results are observed to be very sensitive to these lattice parameters and index contrast. A small variation in these values is found to give rise to huge jumps in the fraction of power received at the output branch. This observation attains significance in light of the fact that it has direct impact on fabrication procedures where often, engineering of such precision structures is formidable, if not infeasible.

Future Research

In this thesis, the optimization work has been performed by trial and error method using the RSOFT software. The recent trend for the optimization is to use some advance methods like topology optimization method using MATLAB, geometry projection optimization method using COMSOL, simulated annealing fabrication technology, etc. In this work, the optimization process will be replaced by the advance methods. Moreover, here the experiment material is gallium arsenide (GaAs) as the background material. Recently more advanced material systems like silicon wafers, photonic crystals made of air spheres in titania (TiO_2) *[28]*, liquid-crystal photonic band gap *[29]*, fabrication of two dimensional high aspect ratio polymer photonic crystal laser *[30]* and many others can be added in PhC analysis. The future plan is to include these modern material systems in the design and analysis.

In various recent works, different types of photonic crystal has been used and proposed. The future aim is to incorporate those photonic crystal arrangements in the design and analysis. For more accurate analysis of a design, it is necessary to include more accurate parameter checking to design future devices with much advanced and impeccable optimizations.

Now-a-days in different structures, PhC is added to suppress the multimode output signal. So, the ultimate goal to design such PhC for the different device structure like Semiconductor Laser, multiple quantum well (MQW) LED etc.

List of references

1) P. I. Borel, A. Harpøth, L. H. Frandsen, M. Kristensen. "Topology optimization and fabrication of photonic crystal structures"2004.

2) Walter R. Frei, Ph.D."Optimization of a Photonic Crystal Waveguide Termination using the Geometry Projection Method and Comsol".

3) Woo Jun Kim and John D. O'Brien, "Optimization of a two-dimensional photonic-crystal waveguide branch by simulated annealing and the finite-element method," J. Opt. Soc. Am. B 21, 289-295 (2004).

4) Esteban Moreno Soriano," MMP Modeling and Optimization of Photonic Crystals, Optical Devices, and Nanostructures".2002.

5) Joannopoulos, J. D., R. D. Meads and J. N. Winn, "Photonic Crystals: Molding the Flow of Light" Princeton University, Princeton, N.J. 1995.

6) Yablonovitch, E., "Inhibited spontaneous emission in solid-state physics and electronics," Physical Review Letters, vol. 58, No. 20, pp. 2059-2062, 1987.

7) John, S., "Strong localization of photons in certain disordered dielectrics super lattices," Physical Review Letters, vol. 58, No. 23, pp. 2486-2489, 1987.

8) E. M. Purcell, "Spontaneous emission probabilities at radio frequencies," Phys. Rev., vol. 69, no. 11-12, p. 681, 1946.

9) V. P. Bykov, \Spontaneous emission in a periodic structure," Soviet Physics JETP, vol. 35, no. 2, pp. 269{273, 1972.

10) Yeh, P., "Optical Waves in Layered Media," John Wiley & Sons, 1988.

11) Villeneuve, P. R., S. Fan, J. D. Joannopoulos, K-Y. Lim, G. S. Petrich, L. A. Kolodziejski, and R. Reif, "Air-bridge microcavities," Applied Physics Letters, vol. 67 (2), pp.167-169, 1995(1).

12) Lourtioz, J.-M., H. Bensity, V. Berger, J.-M. Gerard, D. Maystre, A. Tchelnokov, "Photonic Crystals, Towards Nanoscale Photonic Devices," Springer 2005

13) E. Yablonovitch, "Inhibited spontaneous emission in solid-state physics and electronics," Phys. Rev. Lett. 58, 2059–2062 (1987).

14) K. M. Ho, C. T. Chan, and C. M. Soukoulis, "Existence of a photonic gap in

Periodic dielectric structures," Phys. Rev. Lett. 65, 3152–3155 (1990).

11) E. Yablonovitch and T. J. Gmitter, "Photonic band structure: the face-centeredcubic case," Phys. Rev. Lett. 63, 1950–1953 (1989).

15) K. M. Ho, C. T. Chan, and C. M. Soukoulis, "Existence of a photonic gap in Periodic dielectric structures," Phys. Rev. Lett. 65, 3152–3155 (1990).

16) E. Yablonovitch, T. J. Gmitter, and K. M. Leung, "Photonic band structure: the face-centered-cubic case employing non-spherical atoms," Phys. Rev. Lett. 67, 2295–2298 (1991).

17) C. T. Chan, Q. L. Yu, and K. M. Ho, "Order-N spectral methods for electromagnetic waves," Phys. Rev. B 51, 16635–16642 (1995).

18) Villeneuve, P., S. Fan and J. D. Joannopoulos, "Microcavities in photonic crystals," Microcavities and Photonic Bandgaps: Physics and Applications, NATO ASI Series, Series E: Applied Science, vol. 324, pp. 133-152, 1995(2).

19) R. D. Meade, A. Devenyi, J. D. Joannopoulos, O. L. Alerhand, D. A. Smith, and K. Kash, "Novel applications of photonic bandgap materials: Low-loss bands and high Q cavities," J. Appl. Phys. 75, 4753–4755 (1994).

20) J. D. Joannopoulos, Steven G.Johnson, Joshua N. Winn and Robert D.Meade, Photonic Crystals – Modeling the Flow of Light. 2nd Edition, Princeton University Press, ISBN: 978-0-691-12456-8.

21) Steven G. Johnson and J. D. Joannopoulos, Introduction to Photonic Crystals: Bloch's Theorem, Band Diagrams and Gaps (but no Defects), MIT 3rd February 2003.

22) M. Tinkham, Group Theory and Quantum Mechanics (McGraw-Hill, 1964).

23) K. S. Yee, Numerical solution of initial boundary value problems involving Maxwell's equations in isotropic media, IEEE Transactions on Antennas and Propagation, vol. 14, pp. 302-307, 1966.

24) T. Asano, B. S. Song, and S. Noda, "Analysis of the experimental Q factors (similar to 1 million) of photonic crystal nanocavities," *Optics Express,* vol. 14, pp. 1996-2002, 2006.

25) A. Taflove, Computational Electromagnetics: The Finite-Defference Time-Domain Method (Artech, Boston,Mass., 1995).

26) B.-S. Song, S. Noda, T. Asano, and Y. Akahane, "Ultra-high-Q photonic double heterostructure nanocavity," *Nat Mater,* vol. 4, pp. 207-210, 2005.

27) M. Notomi, E. Kuramochi, H. Taniyama. NTT Basic Research Laboratories, NTT Corporation, Atsugi, Kanagawa 243-0198, Japan, "Ultrahigh-Q Nanocavity with 1D Photonic Gap", Published 21 July 2008 / Vol. 16, No. 15 / Optics Express 11095.

28) Judith E. G. J. Wijnhoven, Willem L. Vos, "Preparation of Photonic Crystals Made of Air Spheres in Titania", Science 7 August 1998: Vol. 281 no. 5378 pp. 802-804, Van der Waals-Zeeman Instituut, Universiteit van Amsterdam, Valckenierstraat 65, NL-1018 XE Amsterdam, Netherlands.http://www.wins.uva.nl/research/scm.

29) Kurt Busch and Sajeev John, "Liquid-Crystal Photonic-Band-Gap Materials: The Tunable Electromagnetic Vacuum", Published 2 August 1999, Volume 83, Number 5, Department of Physics, University of Toronto, 60 St. George Street, Toronto, Ontario, Canada M5S 1A7.

30) Jie Zhou, Gang Liu, Xiaobo Zhang , Xueliang Kang, Ying Xiong, Yangchao Tian, "Fabrication of two dimensional high aspect ratio polymer photonic crystal laser", Microsyst Technol (2013) 19:477–482, Received: 6 August 2011 / Accepted: 27 December 2012 / Published online: 8 January 2013.